Reconnaissance of the Geotechnical and Infrastructure Impacts of Los Angeles Area Wildfires and Subsequent Storms

A report of the NSF-Sponsored Geotechnical Extreme Event Reconnaissance Association

GEER Team Leaders

Idil Deniz Akin, Scott J. Brandenberg, Jonathan P. Stewart; UCLA Engineering

Authors

Idil Deniz Akin, Julio C. Guerra, Steve Zhang, Sera Tirkes, Arda Sahin, John Stapleton, Henry Nagle, Drew Ali, Fatemah Obidan, Debasish Jana, Melis Fidansoy, Timu Gallien, Sriram Narasimhan, Scott J. Brandenberg, Jonathan P. Stewart; UCLA Engineering

Donald Lindsay, David Cavagnaro, Nina Oakley, Derek Cheung, Alex Morelan; California Geological Survey

Kenneth S. Hudson, Martin B. Hudson; Hudson Geotechnics, Inc. and UCLA Engineering

Seulgi Moon, Tyler Horvath, Alexander Koutsoukos, David Paige; UCLA Earth, Planetary, and Space Sciences

Craig Davis; CA Davis Engineering

Michael Lamb, Zhiang Chen, Emily Geyman; California Institute of Technology Division of Geological and Planetary Sciences

Luc Lenain and Gregory Sinnett, Scripps Institution of Oceanography

A. Joshua West and Adit Ghosh; USC Earth Sciences and Environmental Studies

June 13, 2025

Executive Summary

The Palisades and Eaton Fires started on January 7th, 2025 during a major Santa Ana wind storm and burned a total of 15,163 hectares of land until they were fully-contained on January 31st, 2025. Both fires ignited near the wildland-urban interface and spread quickly because of the heavy winds and low humidity, ultimately developing into two of the most devastating conflagrations in California history. The fires caused the deaths of 30 people and combustion of 16,251 structures.

This report summarizes the extensive reconnaissance efforts that started shortly after the fires were contained and field teams could be deployed. The objective of the reconnaissance efforts was to document damage to infrastructure and the natural environment, with a focus on the geotechnical impacts of the wildfires and the temporal evolution of post-fire earth processes generated by three rainstorms on January 25th, February 13th, and March 13th. In addition to field visits to key sites of interest, aerial and ground-based imagery and LiDAR were performed to document damage in the residential and commercial areas and sediment movement in the hillslopes. Field personnel also installed instrumentation and performed field and laboratory measurements to evaluate post-wildfire hydrological changes and changes in surficial soil properties that impact erosional processes and the potential for development of debris flows.

Collectively, the field observations and preliminary image interpretations provide valuable data on the performance of infrastructure elements including water systems, wastewater systems, storm drains, natural gas lines and meters, electric power systems, telecommunication systems, pavement and roadside areas, various types of retaining walls and culverts, and structures. The hillslopes monitoring programs documented post-wildfire soil conditions including burn severity, water repellency, ash thickness, and the presence of macropores. These efforts also evaluated impacts on vegetation and sediment transport processes including dry ravel, rilling, landslides, debris floods/flows after multiple storm events.

Photos, track logs, and shapefiles representing drone flight coverage areas have been published (Akin et al. 2025) via the DesignSafe cyberinfrastructure (Rathje et al. 2017). Furthermore, a map presenting the data can be found at the following URL: https://doi.org/10.17603/ds2-6g0m-xn64. The dataset will likely be amended in the future to include LiDAR point clouds, shapefiles representing aerial LiDAR flight paths, and observations of any future land movements.

The data presented in this report will support future studies of infrastructure system performance and research aimed at developing improved post-wildfire hydrology and sediment movement models. As such, these efforts follow in GEER's long tradition of turning disaster into knowledge.

Acknowledgments

Table of Contents

1.0   Introduction

Two devastating wildfires (Palisades and Eaton Fire) burned a total of 15,163 hectares of land in Los Angeles between January 7 and January 31, 2025. Both fires ignited near the wildland-urban interface and the burn areas include residential and commercial areas in Pacific Palisades, Malibu, Altadena, and Pasadena. Following the fires extensive reconnaissance efforts were initiated that included multiple teams investigating the impacts of these wildfires on the built and natural environments. The objective of this report is to summarize the scope and findings of these reconnaissance efforts, with a particular focus on the geotechnical impacts of these wildfires.

1.1. Event Overview

The greater Los Angeles region experienced two large fires that ignited on January 7th, 2025. The Palisades Fire burned 23,448 acres and the Eaton Fire burned 14,021 acres of land before they were contained on January 31st, 2025. The Palisades Fire directly affected Pacific Palisades (zip code 90272) and Malibu (zip code 90265) and the Eaton Fire affected Altadena and Pasadena (zip code 91001). To date, at least 30 people lost their lives (12 in the Palisades Fire and 18 in the Eaton Fire). A total of 16,251 structures (6,833 in Palisades Fire) were destroyed, 2,046 structures (973 in Palisades Fire) were damaged, and 12,372 structures (12,312 in Palisades Fire) were threatened. The total economic loss due to the LA Fires, including the insured and uninsured property losses, losses due to damaged infrastructure, and environmental and cleanup costs, is estimated to be between $76 billion and $131 billion. Among those losses, the insured loss amounts are estimated to be between $20 billion and $45 billion (Li and Yu 2025).

The Palisades Fire started around 10:30 am on the Temescal Ridge Trail, southeast of Palisades Drive in Pacific Palisades. By noon, evacuation orders were placed in the majority of Pacific Palisades. The fire spread quickly toward Sunset Mesa to the south and Malibu to the west because of strong Santa Ana winds. By 1:30 pm, the evacuation orders were expanded further east to Brentwood. In the evening on January 7th, the fire moved further north and east and evacuation orders were expanded to Santa Monica to the east and Topanga to the north. The fire mainly progressed to the north on the remaining days (Fig. 1.1).

The Eaton Fire started on the evening of January 7th, 2025, near Altadena Drive and Midwick Drive in the community of Altadena. The wind-driven fire spread quickly to the west into Altadena and to the east into Sierra Madre and Arcadia (Fig. 1.2). By the morning of January 8, over 50,000 residents were placed under evacuation orders and over 20,000 were placed under evacuation warnings. The fire primarily progressed northward on the remaining days.
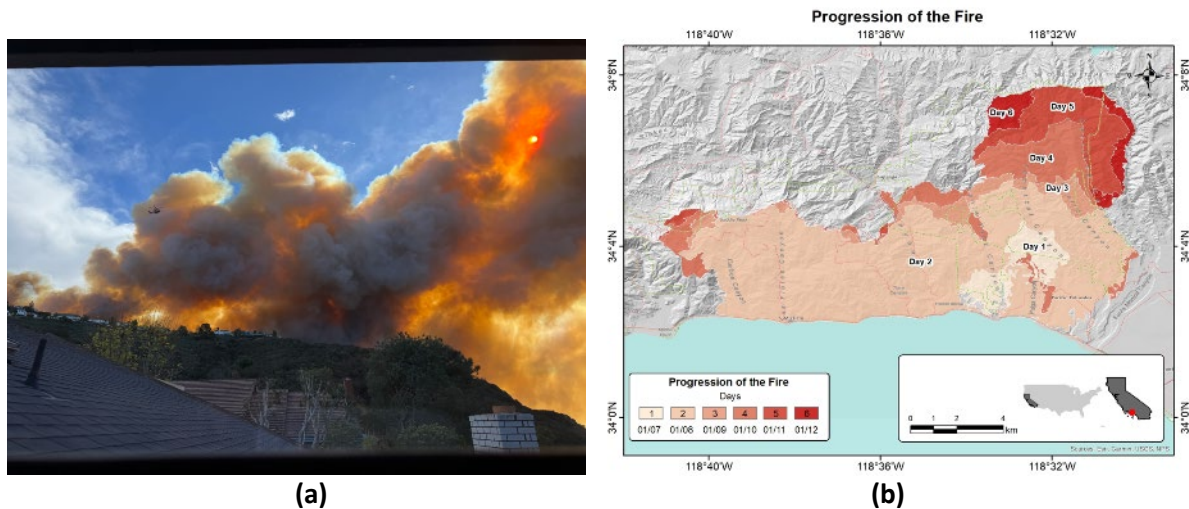
Fig. 1.1. (a) First hour (photo credit: Stephanie Wonser) and (b) day-by-day progression of the Palisades Fire
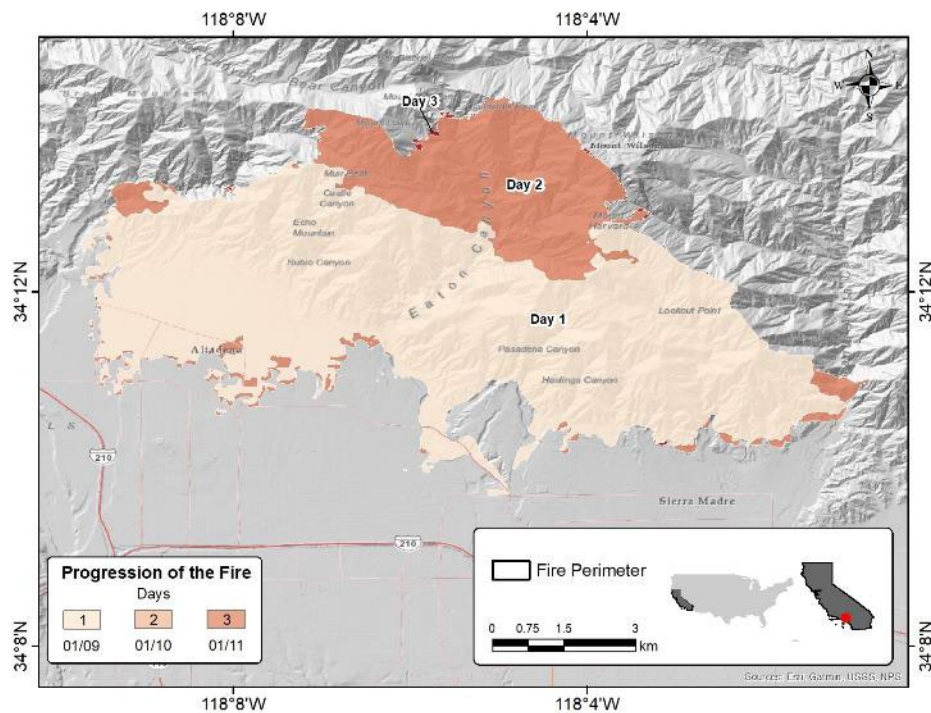
Fig. 1.2. Day-by-day progression of the Eaton Fire.

1.2. Reconnaissance response

In the days following the onset of the fires, consideration was given to how GEER could most effectively respond to the disaster. Not surprisingly for an event of this magnitude, many entities were involved in responding in different ways. GEER leadership sought to track these activities, established partnerships over time with critical (and willing) collaborators, and performed targeted investigations to address critical data gaps. There were significant logistical challenges to access sites in the affected regions because of the large-scale devastation, emergency

7

response efforts, burned houses being treated as potential crime scenes, environmental contamination, and safety and looting concerns. To date, access is still limited in some areas. Because of these logistical challenges, GEER did not issue a solicitation to form a large-scale reconnaissance team, as is often done after extreme events. Rather, the GEER leadership team invited research groups from many different organizations, whose work was performed largely independently, to contribute to this report. The combined contributions of these groups have been collated in this report to provide as comprehensive an overview of the event as practical given the information collected to date. An overview of the scope of those efforts is provided in Section 1.3.

We are aware of additional work performed by other research groups that are not represented in this GEER report. NV5, funded by ALERT California at UC San Diego collected LiDAR data between January 21st and 22nd in partnership with USGS. The DTMs and DSMs were published by USGS (3D Elevation Program 2025). The US Army Corps of Engineers (USACE) was tasked by the California Department of Water Resources to assess the increased post-fire flood risk. Work performed by USACE was completed under the authority of PL 84-99, Flood Control and Coastal Emergencies (FCCE) (33 U.S.C. 701n)(69 Stat.186) for emergency management activities and included conducting a comprehensive hydrologic and hydraulic (H&H) analysis of the burned watersheds, utilizing advanced modeling techniques (Hydrologic Engineering Center's Hydrologic Modeling System, HEC-HMS, and River Analysis System, HEC-RAS) to predict post-fire runoff, debris flow potential, and inundation extents. Prof. Ertugrul Taciroglu received an NSF RAPID grant to study the structural damage after the Palisades and Eaton Fire. Prof. Jennifer Jay, in collaboration with Heal the Bay, investigated post-wildfire water quality in Santa Monica Bay. Prof. Sanjay Mohanty offered free soil testing to homeowners to identify heavy metals, PFAS, and other hazardous contaminants. Prof. Mekonnen Gebremichael received an NSF award to study post-wildfire hydrology. Prof. Jiaqi Ma worked with USACE to optimize debris removal.

1.3. Scope of present field investigations and report organization

1.3.1. Aerial Reconnaissance Missions

A summary of the aerial imagery and LiDAR collections are provided in Table 1.1 and Fig. 1.3 shows the spatial extent of the aerial data collections over the Palisades Fire and Eaton Fire areas. Additional imaging work included high resolution surveys of Topanga and Mandeville Canyons (Palisades Fire) and debris basins (Eaton Fire) using a DJI Zenmuse L2 lidar sensor mounted on a DJI Matrice 350 RTK (dates are marked in Table 1.2).

The Scripps Institution of Oceanography (SIO) Air-Sea Interaction Lab collected point cloud data using a Riegl VQ-780 II-S scanning lidar operating at a 2MHz laser pulse rate with a roughly 20 cm ground sampling distance and a systematic flight line spacing with nominal 50% cross track

overlap. The number of LiDAR returns was 14,836,929,754 for the Palisades flight and 6,976,945,982 for the Eaton flight. Images were captured with a Nikon D850 46 mpx digital single lens reflex (DSLR) nadir camera at a three second period with approximately 7.5 cm ground sample distance. Flight lines were spaced to allow for a nominal 55% horizontal image overlap. LiDAR data was processed to produce a 1 m resolution DTM covering the entire affected area. Additional surface model products up to 0.2 m resolution DTMs were produced at specific sites of interest.
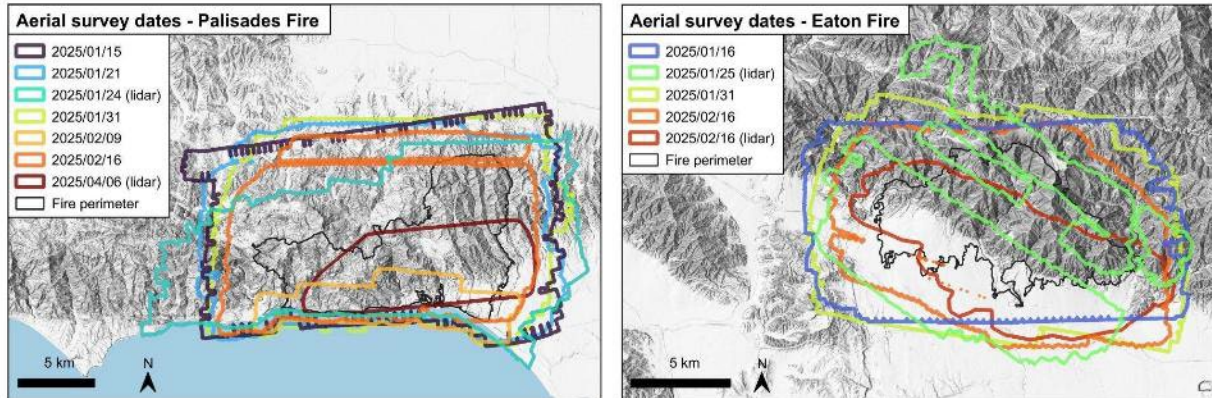
Fig. 1.3. FIRIS and Scripps aerial survey dates and spatial extents over the Palisades Fire and Eaton Fire.

Table 1.1. Summary of the aerial data collection missions.

Collection Date	Collected By	Sensor	Fire Name	Product	Spatial Resolution [cm]	Coverage area [km²]	# of Frames	Point density [m⁻²]
1/15/25	FIRIS	TK	Palisades	SfM DSM	70.2	306.15	1520	
1/15/25	FIRIS	TK	Palisades	Orthomosaic	17.6	306.15	1520	
1/16/25	FIRIS	TK	Eaton	SfM DSM	51.9	179.55	3556	
1/16/25	FIRIS	TK	Eaton	Orthomosaic	13	179.55	3556	
1/21/25	FIRIS	TK	Palisades	SfM DSM	63	296.65	4634	
1/21/25	FIRIS	TK	Palisades	Orthomosaic	15.8	296.65	4634	
1/24/25	SIO	Riegl	Palisades	LiDAR	19.5	262.13		56.6
1/24/25	SIO	Riegl	Palisades	LiDAR DSM	20	Variable		
1/25/25	SIO	Riegl	Eaton	LiDAR	21.5	165.24		42.22
1/25/25	SIO	Riegl	Eaton	LiDAR DSM	100	165.24		
1/31/25	FIRIS	TK	Palisades	SfM DSM	19.7	298.82	2680	
1/31/25	FIRIS	TK	Palisades	Orthomosaic	19.7	298.82	2680	
1/31/25	FIRIS	TK	Eaton	SfM DSM	59.9	198.34	3063	
1/31/25	FIRIS	TK	Eaton	Orthomosaic	15	198.34	3063	
2/9/25	FIRIS	TK	Palisades	SfM DSM	69.2	48.64	976	
2/9/25	FIRIS	TK	Palisades	Orthomosaic	17.3	48.64	976	
2/16/25	FIRIS	TK	Palisades	SfM DSM	39.8	229.85	7621	
2/16/25	FIRIS	TK	Palisades	Orthomosaic	9.94	229.85	7621	
2/16/25	FIRIS	TK	Eaton	SfM DSM	41	155.07	4881	
2/16/25	FIRIS	TK	Eaton	Orthomosaic	10.3	155.07	4881	
2/16/25	FIRIS	LiDAR	Eaton	Bare Earth DTM	50	81.04		7.65
4/6/25	FIRIS	LiDAR	Palisades	Bare Earth DTM	50	69.45		20.905

1.3.2. Ground-Based Reconnaissance Missions

Reconnaissance teams visited the burn areas multiple times after securing permissions from the relevant government agencies (Table 1.2) for scouting, observations, imaging, sampling, testing, and instrumentation. Fig. 1.4 shows the areas the teams visited for the reconnaissance work, along with the drone- and ground-based LiDAR coverage areas.

Several researchers worked on the different aspects of the fires, which contributed to the information presented in this report. CGS, along with its partner CAL FIRE, conducted Watershed Emergency Response Team (WERT) assessments on the Palisades and Eaton Fires. Results of the WERT assessments were presented to federal, state, and local government agencies with the intent to help communities prepare their response by documenting and communicating postfire risks to life, property, and infrastructure posed by debris flow, flood, and rockfall hazards. Both

WERT reports were made publicly available on the CGS' Burned Watershed Geohazards Webpage: https://www.conservation.ca.gov/cgs/bwg/recent. Following the WERT assessment, CGS transitioned to conducting postfire monitoring with federal partners, including the United States Forest Service (USFS) and the United States Geological Survey (USGS), and with academic institutions, including Caltech, UCLA, and USC.

The UCLA team's efforts concentrated on the Palisades Fire because of the team members' familiarity with and proximity to the area. Caltech, USC, and CGS, along with their partners at the USFS and the USGS, focused on the Eaton Fire due to the area's rich historic record of experiencing significant post-fire responses within steep, sediment-rich channels draining the San Gabriel Mountains (Cannon et al. 2008, 2010; Staley et al 2016), the perceived high hazard to downslope communities built on mapped alluvial fan surfaces or along incised channels at the foot of the San Gabriel Mountains, and on the favorable conditions associated with access, property ownership, and proximity to resources that provided a desirable backdrop to conduct post-fire monitoring.

Ground-based surveys were conducted at Palisades Highlands, Temescal Canyon Road, and the Pacific Coast Highway corridor using a survey vehicle outfitted with a roof-mounted Kaarta Stencil Pro mobile mapping system, which integrates lidar, panoramic cameras, and GPS for high-resolution spatial data collection. Efforts were concentrated in residential areas (and Piedra Gorda Canyon/Big Rock, Palisades Highlands/Via Las Palmas, and Surfview Drive) to document damage to infrastructure systems and retaining walls; and in Mandeville, Topanga, and Los Leones Canyons to monitor post-wildfire erosion and assess slope stability issues (i.e., rill erosion, landslides, debris flows). In addition, the Castellammare area was visited multiple times to document a landslide that took place on January 16th, 2025. Sampling and testing at the Palisades site included ash sampling; soil sampling from the surface, 10 cm, 30 cm, and 60 cm depths; and mini disk infiltrometer testing. Instrumentation included soil water content and matric suction sensors, rain gauges, and debris flow monitoring stations. Additionally, electrical Resistivity Tomography (ERT) was conducted at Mandeville (two sites), Rustic, Santa Ynez, Parker Mesa, and Topanga Canyons to monitor changes to groundwater infiltration, in addition to detrital sediment collection for ^{10}Be analysis. In addition, water isotopes (hydrogen and oxygen isotopes) of rainwater and streamwater were collected from Mandeville and Topanga Canyon for all major storms during the winter of 2025 (e.g., 2/13, 3/13) and for a few smaller storms. These samples were collected at a high temporal resolution (~every 30 minutes) throughout the duration of the storm. This data was used to quantify the contribution of 'isotopically young' rainwater relative to 'isotopically old' groundwater in streamflow.

The Scripps Institution of Oceanography Air-Sea Interaction Lab flew a fixed wing aircraft over the Eaton and Palisades fire areas to collect LiDAR, visual imagery, hyperspectral imagery, and IR data in collaboration with UCLA Civil & Environmental Engineering (CEE) faculty. Prof.

Narasimhan's research group conducted infrastructure assessments using field mapping equipment. Prof. Idil Akin received a UCLA rapid grant to monitor post-wildfire hydrology and landslide susceptibility. Prof. Moon, Meng, Prof. Paige, and EPSS department received a donation from William Schopf and Michael Thacher for field instrumentations for post-debris flow monitoring. Prof. West received support from the Center for Land Surface Hazards. Prof. Timu Gallien collected Acoustic Doppler Current Profiler data offshore during the fires and received a UCLA rapid grant to collect eDNA from near the breakwater to understand the impact of the Palisades Fire on urban marine life in the Santa Monica Bay.

As part of the WERT assessment and the post-February storm response assessment, CGS requested high-resolution imagery that was collected by the California Office of Emergency Services (CalOES) and Fire Integrated Real-time Intelligence System (FIRIS) program. Using the FIRIS overlapping aerial imagery, CGS employed digital photogrammetry software called Agisoft Metashape to generate digital surface models (DSMs) and orthomosaics. The CalOES FIRIS aircraft also performed lidar collection, which involves a sensor that emits laser pulses towards the ground and measures the reflected returns to accurately capture detailed elevation and terrain features. LiDAR provides precise three-dimensional data, which is useful for analyzing the changing landscape conditions, vegetation structure, and built environments. These data significantly enhance emergency planning, hazard modeling, and infrastructure assessment capabilities. CGS was provided an unclassified point cloud from which they extracted ground points and produced a bare-earth digital terrain model (DTM).

At the Eaton Fire site, reconnaissance efforts were concentrated in the debris basins to monitor select debris basin capacities after the fire, after subsequent rain events, and after LA County clean-out efforts. CGS installed a telemetered weather station at the watershed divide above Bailey Canyon, a non-contact stage recorder, geophone array and a game camera within Stonehill Canyon, and a non-contact stage and velocity recorder, geophone array, and game camera within Pasadena Canyon (Fig. 1.4).

The team will continue to make field measurements and near-surface geophysical surveys to document the evolution of post-fire earth processes.

Table 1.2. Field visit dates, objectives, locations. [1-27]mission numbers, *LiDAR drone flight dates.

Mission	Fire	Date	Objective	Location
1	Palisades	1/22/25	Infrastructure assessment using the mobile mapping system	Pacific Coast Hwy, West Sunset Blvd, Palisades Dr and surrounding communities
2	Palisades	1/13-20/25	Field work for the Palisades Fire WERT assessment	Mandeville, Topanga, Santa Ynez, Tuna, Temescal Canyons and surrounding communities
3	Eaton	1/16-24/25	Field work for the Eaton Fire WERT assessment	Altadena, Arcadia, Pasadena Glen, Sierra Madre and surrounding communities
4	Palisades	1/26/25	Water isotope samples	Mandeville Canyon
5	Palisades	2/4/25	Scouting, sampling, testing	Mandeville Canyon, Los Liones Dr, Surfview Dr, Piedra Gorda Canyon/Big Rock, Palisades Highlands/Via Las Palmas, Castellammare
6	Palisades	2/5/25	Water isotope samples	Mandeville Canyon
7	Palisades	2/8/25	Scouting, post-storm/pre-storm reconnaissance	Palisades Highlands/Via Las Palmas Castellammare Piedra Gorda Canyon/Big Rock
8	Palisades	2/11-12/25	Pre-storm reconnaissance, sampling, testing, instrumentation	Mandeville (*1) and Topanga Canyons (*1)
9	Palisades	2/13/25	Water isotope sampling during storm	Mandeville Canyon, Topanga Canyon
10	Palisades	2/18-19/25	Post-storm reconnaissance	Mandeville Canyon (*2), Los Leones Dr, Topanga Canyon
11	Eaton	2/19-21/25	Post-storm reconnaissance Monitoring equipment installation.	Rubio Canyon, Stonehill Canyon, Bailey Canyon, Pasadena Glen
12	Palisades	2/23/25	Post-storm reconnaissance	Piedra Gorda Canyon/Big Rock, Palisades Highlands/Via Las Palmas, Castellammare
13	Palisades	3/5/25	Water isotope sampling during storm	Mandeville and Topanga Canyons
14	Palisades	3/6/25	Sampling, testing, instrumentation	Mandeville Canyon
15	Palisades	3/7/25	Scouting, sampling, testing, instrumentation Post-storm reconnaissance	Los Leones Dr, Topanga Canyon (*2)
16	Palisades	3/7/25	ERT	Mandeville Canyon
17	Palisades	3/8/25	ERT	Topanga Canyon
18	Palisades	3/13/25	ERT	Mandeville and Topanga Canyons
19	Palisades	3/18/25	Sampling, testing, instrumentation	Mandeville Canyon
20	Palisades	3/22/25	Post-storm reconnaissance	Topanga Canyon (*3)
21	Palisades	3/26-27/25	Scouting, sampling, testing, instrumentation	Topanga Canyon
22	Palisades	4/1/25	Post-storm reconnaissance	Castellammare, Mandeville Canyon (*3)
23	Palisades	4/6/25	ERT	Mandeville Canyon
24	Palisades	4/7/25	ERT	Topanga Canyon, Parker Mesa
25	Palisades	4/8/25	ERT	Rustic Canyon, Santa Ynez Canyon
26	Palisades	5/15/25	ERT, sampling, testing, instrumentation	Mandeville Canyon
27	Palisades	5/18/25	ERT	Rustic Canyon, Topanga Canyon, Parker Mesa, Santa Ynez Canyon

Fig. 1.4. Monitoring Stations map for the Palisades Fire and Eaton Fire

2.0 Palisades Fire

2.1. Geology

The Palisades Burn area is in the southeastern portion of the Santa Monica Mountains, within the Western Transverse Ranges. These ranges contain several east-west trending mountain ranges including the Santa Ynez, Santa Monica, and San Gabriel Mountains. The Western Transverse Ranges are bounded on the south by the Peninsular Ranges province and on the north by the Coast Ranges province. The Palisades Burn area primarily consists of marine sedimentary rocks ranging in age from the Cretaceous to the Miocene, as well as Miocene volcanic and volcaniclastic rocks (Fig. 2.1).

Fig. 2.1. Geology of the Palisades burn area.

Geologic Map Units - Palisades Fire

Late Holocene (Surficial Deposits)

af	Artificial fill
Qsu	Undifferentiated Surficial Deposits
Qls	Landslide deposits
Qb	Beach deposits
Qw	Alluvial wash deposits
Qf	Alluvial fan deposits
Qa	Alluvial valley deposits

Holocene to Late Pleistocene (Surficial Deposits)

Qyf	Young alluvial fan deposits
Qya	Young alluvial valley deposits

Late to Middle Pleistocene (Surficial Deposits)

Qof	Old alluvial fan deposits
Qoa	Old alluvial valley deposits
Qol	Old Lacustrine, Playa, and Estuarine (Paralic) Deposits

Tertiary (Bedrock)

Tss	Coarse-grained Tertiary age formations
Tsh	Fine-grained Tertiary age formations
Tv	Tertiary age formations of volcanic origin

Mesozoic and Older (Bedrock)

Kss	Coarse-grained Cretaceous age formations of sedimentary origin
Ksh	Fine-grained Cretaceous age formations of sedimentary origin
pKm	Cretaceous and pre-Cretaceous metamorphic formations of sedimentary and volcanic origin
gr	Granitic and other intrusive crystalline rocks of all ages

MAP SYMBOLS

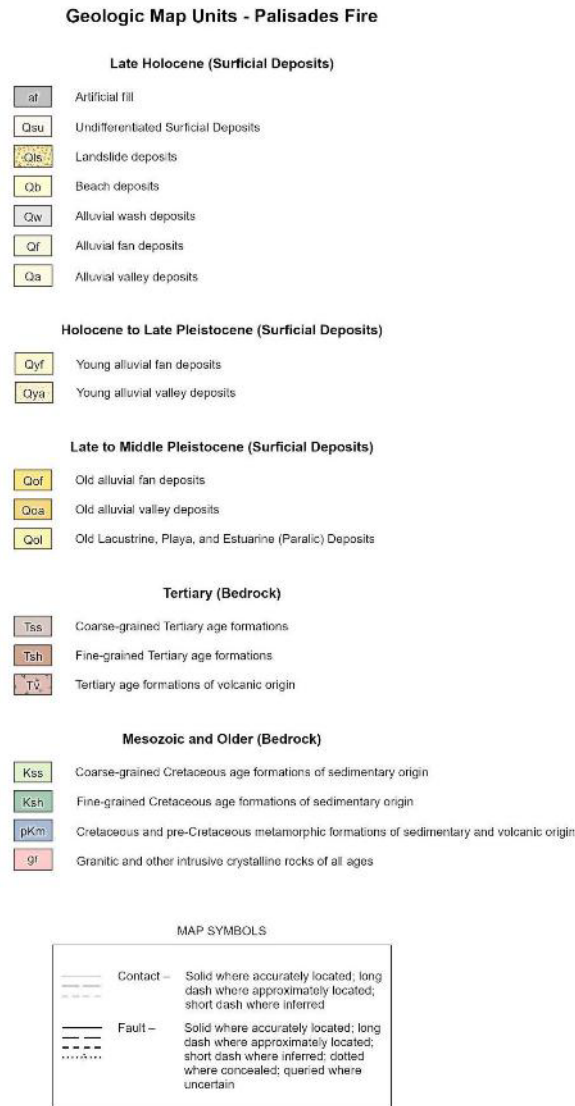|		
	Contact –	Solid where accurately located; long dash where approximately located; short dash where inferred
	Fault –	Solid where accurately located; long dash where approximately located; short dash where inferred; dotted where concealed; queried where uncertain

Fig. 2.1 (continued). Description of geologic map units for the Palisades burn area.

These units overlie older Jurassic metamorphic rocks in the eastern part of the region (Yerkes and Campbell 1979, Dibblee 1982). During the Miocene, the Western Transverse Ranges experienced approximately 90° of clockwise rotation and transtensional deformation, resulting in the accumulation of thick sequences of marine sandstones, marine siliceous mudstones, and volcaniclastic rocks (Atwater 1998, Namson and Davis 1988). These sedimentary units were subsequently deformed into an east–west-trending anticlinorium that defines the modern Santa Monica Mountains, bounded to the south by the Malibu Coast fault (Davis & Namson, 1994). Tectonic uplift rates along the Malibu Coast fault are estimated to range from 0.1 to 0.4 mm/yr based on paleoseismic and neotectonic studies (e.g., Dolan et al. 2000), and up to ~1 mm/yr based on llow temperaturethermochronology (Niemi and Clark 2017, Townsend et al. 2021).

2.2. History of regional fires, landslides, and debris flows

The Santa Monica Mountains are coastal mountains that parallel the Pacific Coast in Southern California and have historically seen multiple small- and large-scale wildfires (Fig. 2.2). The most recent notable fire before the Palisades Fire was the 2018 Woolsey Fire, which burned 96,949 acres of land between November 8th, 2018 and January 4th, 2019. The most recent event before the Palisades Fire was the 2024 Franklin Fire, which burned 4,037 acres of land between December 9th, 2024 and December 18th, 2024.
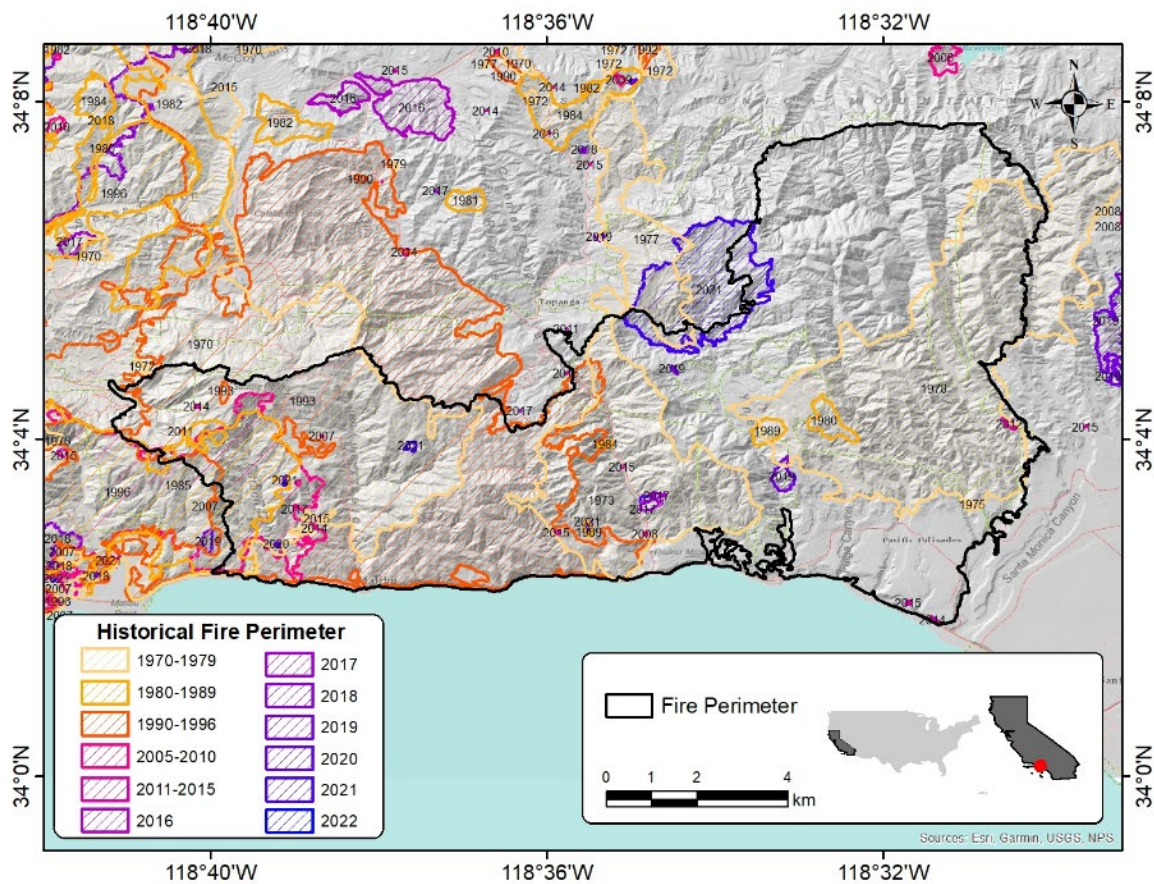

Fig. 2.2. Palisades Fire perimeter (black) and historic wildfire perimeters in the surrounding area

The steep slopes in the area burned by the Palisades Fire have historically been prone to landslides (Fig. 2.3). Slope instability evaluation and stabilization in the Palisades Fire burn area are discussed by URS (2010), Buckley and Hollingsworth (1984), and Krohn (1992). The landslides have included deep-seated rapid failures, deep-seated creep-type movements, and long-term and short-term shallow landslides. The slopes are composed of a variety of geologic materials ranging from loose to engineered fill, alluvium/colluvium, and formational materials consisting of conglomerate, shale, sandstone, siltstone, and claystone, many of which are soft, with

numerous areas that include adversely bedded shale and clay layers that contribute to instability. There are numerous faults through the area with associated planes of weakness that can contribute to slope instability. There is much natural instability that can be observed, as well as instability due to development of the area which resulted in cuts at the base of hills, fills on slopes, alteration of drainage patterns, and increase of groundwater due to irrigation of residential and commercial properties. There have been many landslide stabilization measures taken over the last 100 years in response to slope instability events, including retaining structures (conventional retaining walls, mechanically stabilized earth systems, and temporary and permanent tie-back anchor restrained systems), drainage measures including hydraugers, surface drainage improvements, regrading, and surficial stabilization such as plastic sheeting over slopes, geosynthetic surficial stabilization, and hydroseeding.
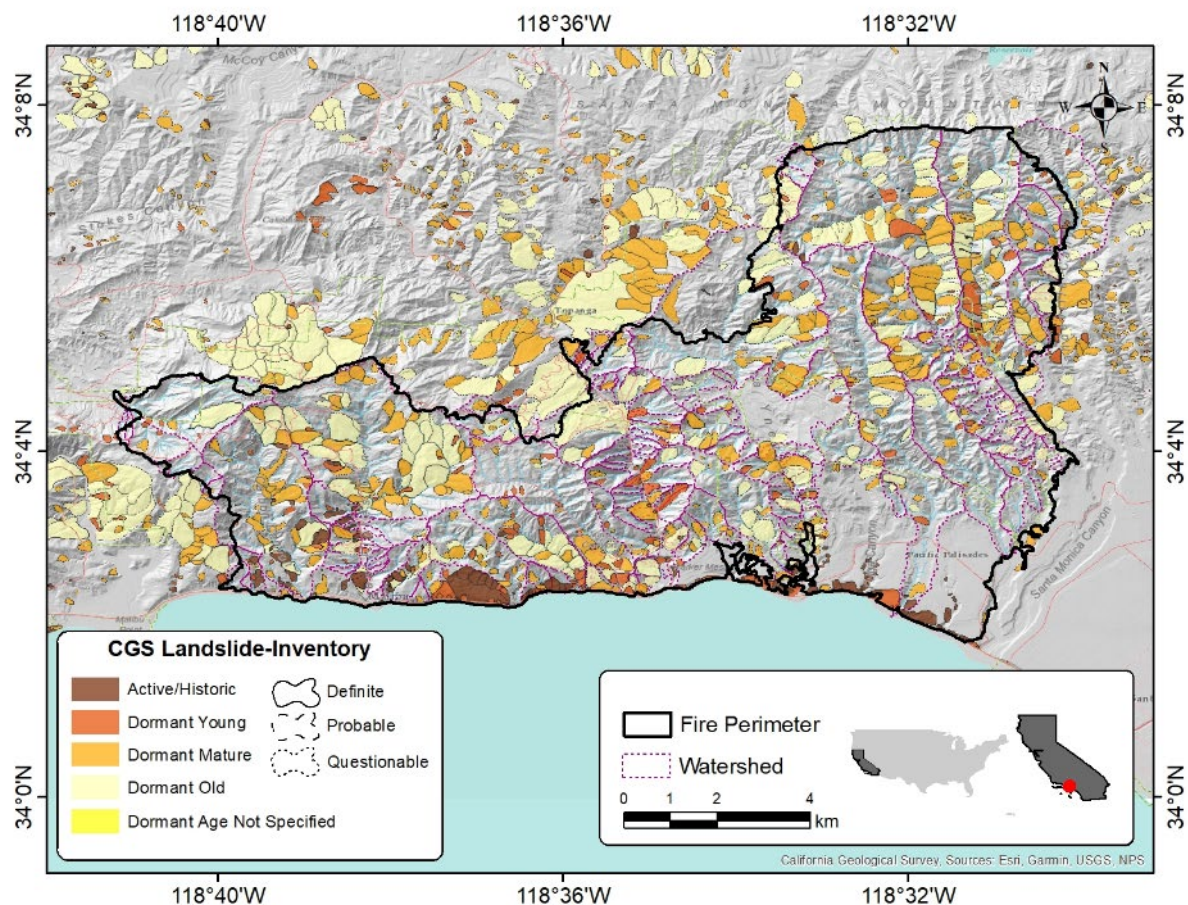

Fig. 2.3. Historic landslide activity within the Palisades Fire burn perimeter and the surrounding area

Shallow translational landslide failures, referred to as soil slips (Bailey, 1969), are common in the Santa Monica Mountains, particularly after large storms generate excessive pore water pressures

18

within the upper soil profile causing mass failure of colluvial soil cover of steep hillsides and colluvial fill in steep ravines (Campbell 1975). In some cases, soil slips transition into debris flows as they progress downgradient within confined channels. Extensive soil slips were documented impacting areas within Topanga Canyon and nearby hills following record-setting rainfall between January 18 and 26, 1969 (Campbell 1975).

Following wildfire, postfire hazards have a tendency to transition from being runoff-dominated flood and debris flow hazards to more infiltration-generated landslide hazards starting 3 to 5 years following fire (Rice and Foggin 1971, Rengers et al. 2020). This increase in landslide activity, particularly shallow soil slip failures, can be attributed to a reduction in root strength (Vergani et al. 2017) and altered surface and shallow subsurface hydrology. Recent unpublished mapping performed by CGS shows an increase in shallow landsliding within the Santa Monica Mountains following the 2018 Woolsey Fire that was triggered by a heavy storm on December 30th, 2021, approximately 3.5 years after the fire. Although similar landslides occurred on unburned slopes in the region, satellite imagery shows that the landslide density within the Woolsey burn scar appears to be greater.

2.3. Site selection

The reconnaissance efforts in the Palisades Fire focused on (1) the Pacific Palisades to document the damage to infrastructure, (2) Mandeville, Los Leones, and Topanga Canyons to evaluate post-wildfire slope stability issues, and (3) the Castellammare area to document a landslide that occurred in January, before the fire was fully contained. The mountainous sites were selected based on access and debris flow and landslide risk. The teams got early access to Mandeville and Los Leones Canyons through the LA Bureau of Engineering, shortly after the fire was contained and access restrictions were reduced. Topanga Canyon was selected based on the USGS debris flow model (Fig. 2.4, Staley et al. 2017). The small, steep watersheds within the canyon are classified as having high potential for post-fire debris flow activity. Our team conducted multiple site visits before and after major storms with the assistance of Caltrans and Topanga State Park.

The sites for ERT and [10]Be analysis were selected based on gradient in topography and rilling intensity. Mandeville and Rustic Canyons in the eastern portion of the study area are characterized by gentler topography, while the Western sites- Santa Ynez, Parker Mesa and Topanga lie in steeper terrain. Rilling was most prominently developed at Parker Mesa and Topanga Canyon.
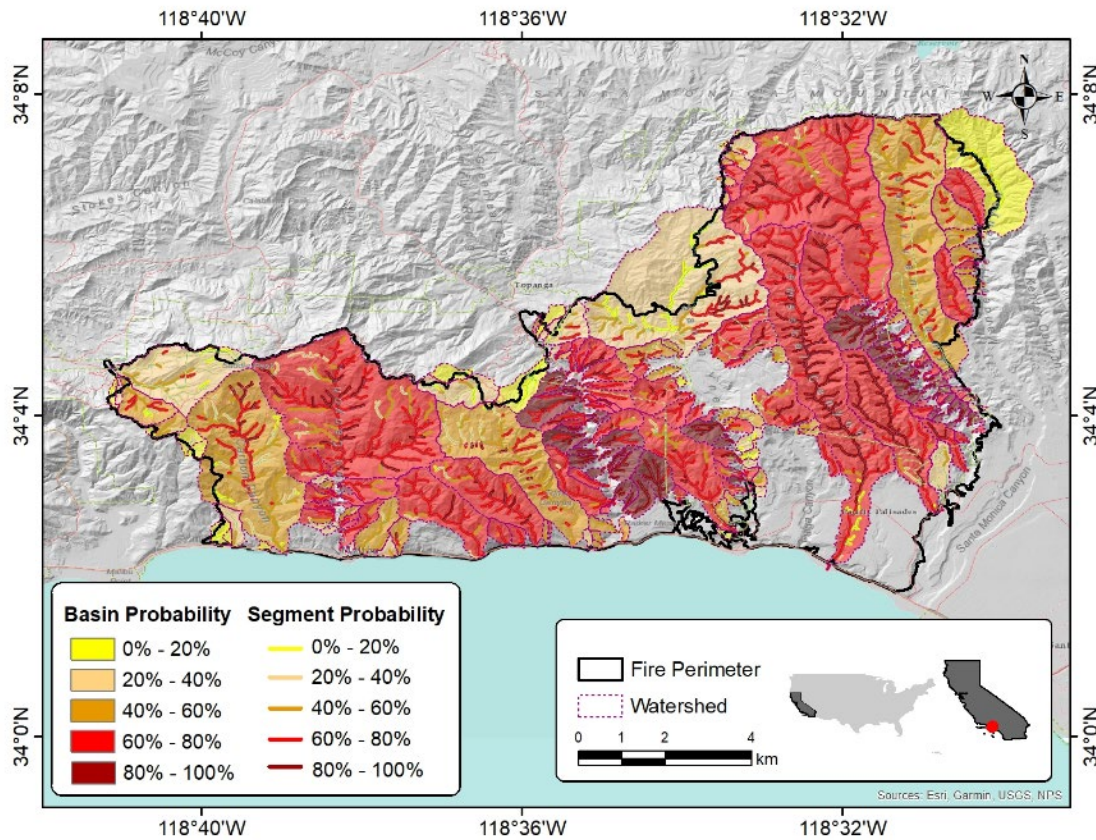
Fig. 2.4. Debris flow likelihood at the Palisades Fire (24 mm/h storm) according to USGS debris flow model (Staley et al. 2017).

2.4. Imaging

High resolution surveys of Mandeville and Topanga Canyons were conducted with a DJI Matrice 350 RTK, an unpiloted aerial vehicle equipped with real-time kinematic capabilities (Fig. 2.5). Mounted on the UAV was the DJI Zenmuse L2 lidar sensor, a high-resolution system optimized for detailed topographic mapping and terrain modeling. The DJI RTK 2 system was used for RTK corrections. The UAV system was operated with four pairs of TB65 batteries, and the batteries were charged using a car-based power inverter. Surveys were conducted at flight altitudes between 100 and 120 m above ground level, employing the UAV's terrain-following feature to maintain a consistent ground sampling resolution. This approach achieved a spatial resolution of approximately 3.5 cm per pixel and yielded point densities ranging from 500 to 700 points per square meter. An 80% front overlap and a 20% lateral overlap was established between data frames to ensure sufficient coverage and minimize data gaps. RGB imaging was enabled during the flights, providing color information for point cloud visualization. The UAV operated at a

maximum speed of 15 m/s, with an average survey speed maintained at approximately 6 m/s to optimize data quality.

Fig. 2.5. Unpiloted aerial vehicle carrying a lidar sensor system used for high-resolution post-fire topographic mapping.

The ground-based surveys were conducted using a Kaarta Stencil Pro mobile mapping system (Fig. 2.6a). The system integrates a Velodyne VLP-32C lidar sensor, capable of capturing 600,000 points per second across distances of up to 120 meters, generating dense 3D point clouds of terrain and infrastructure. It also includes four 8-megapixel 4K panoramic color cameras that capture 360-degree imagery, allowing for colorized point cloud generation and detailed visual documentation.

| (a) | (b) |
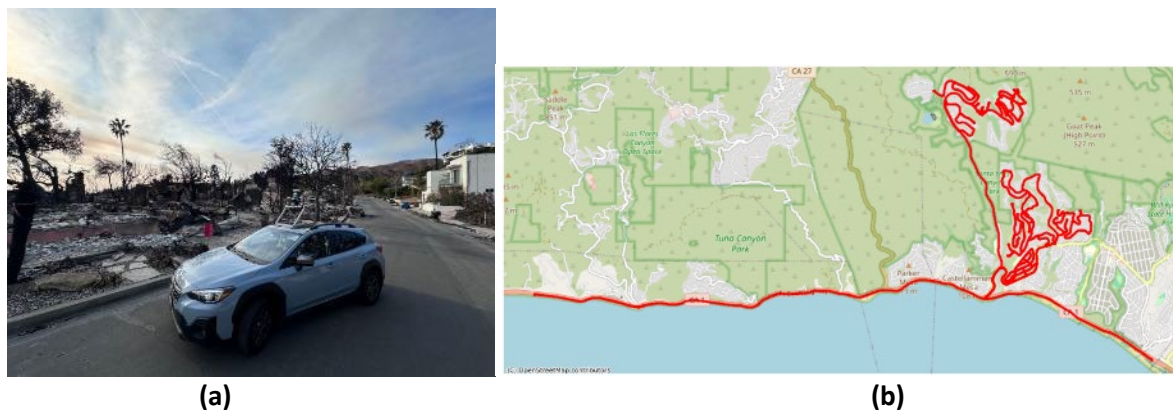
Fig. 2.6. (a) The Kaarta Stencil Pro mobile mapping system and (b) transverse routes.

The mobile mapping surveys were conducted across three wildfire-impacted areas (Fig. 2.6b) to evaluate post-fire damage and infrastructure vulnerability. The survey covered (1) the Palisades Highlands neighborhood, where we assessed slope stability, retaining wall conditions, and structural damage in densely built hillside communities; (2) Temescal Canyon Road, a critical north-south corridor used for emergency access and evacuation, where we documented debris flood/flow and burn scars along the steep slopes; and (3) a segment of the Pacific Coast Highway

(PCH), a key arterial route running along the coastline, where we recorded impacts to retaining structures, slope faces, and roadside utilities. These areas were prioritized due to their proximity to the wildland-urban interface and their significance for regional mobility, emergency response, and public safety.

Aerial surveys flown by fixed wing aircraft were conducted across Eaton and Palisades wildfire-impacted areas. The Scripps Institution of Oceanography Modular Aerial Sensing System (MASS, Fig. 2.7) was used to collect LiDAR, imagery, hyperspectral and IR data. The MASS is a portable package of high-resolution instrumentation built specifically for airborne remote sensing applications. Instrumentation includes an airborne topographic LiDAR integrated with infrared, RGB and hyperspectral imaging systems. The system is coupled to a highly accurate GPS-aided inertial measurement unit (GPS IMU), permitting co-located airborne measurements of terrain, vegetation and structures. LiDAR products over the burn area consist of surface terrain models and classified LiDAR point clouds (Fig. 2.8).

Fig. 2.7 Aircraft-mounted Modular Aerial Sensing System used to survey the Eaton and Palisades fire areas. Instruments consist of IMU, LiDAR, and IR, Hyperspectral, and RGB cameras.
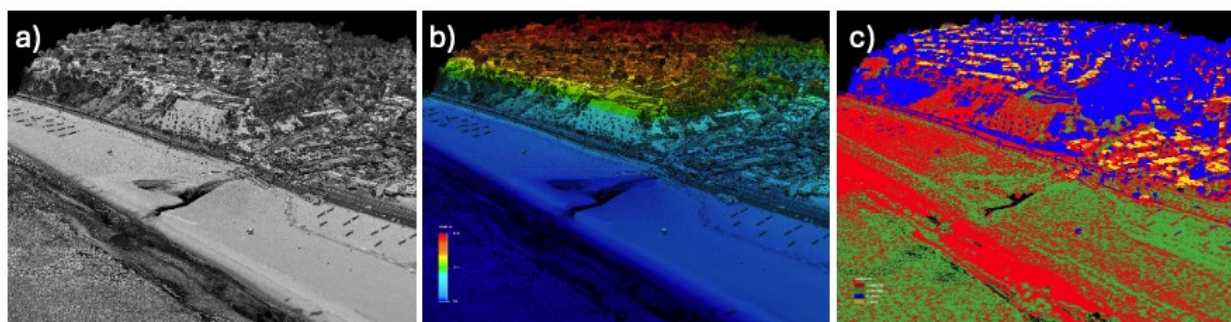

Fig. 2.8 Example LiDAR products over the Chautauqua drain area (part of the affected Palisades burn area). The a) LiDAR intensity, b) surface elevation, and c) classified LiDAR point cloud are used to define surface properties. LiDAR classifications in c) include ground (green), buildings (yellow), vegetation (blue) and other (red).

2.5. Soil burn severity, composition, and vegetation

The majority (51%) of the slopes within the Palisades Fire burn perimeter were classified as moderate soil burn severity, with 3% high severity, 31% low severity, 2% unburned to low soil burn severity, and 13% being developed land (Watershed Emergency Response Team 2025, Fig. 2.9).
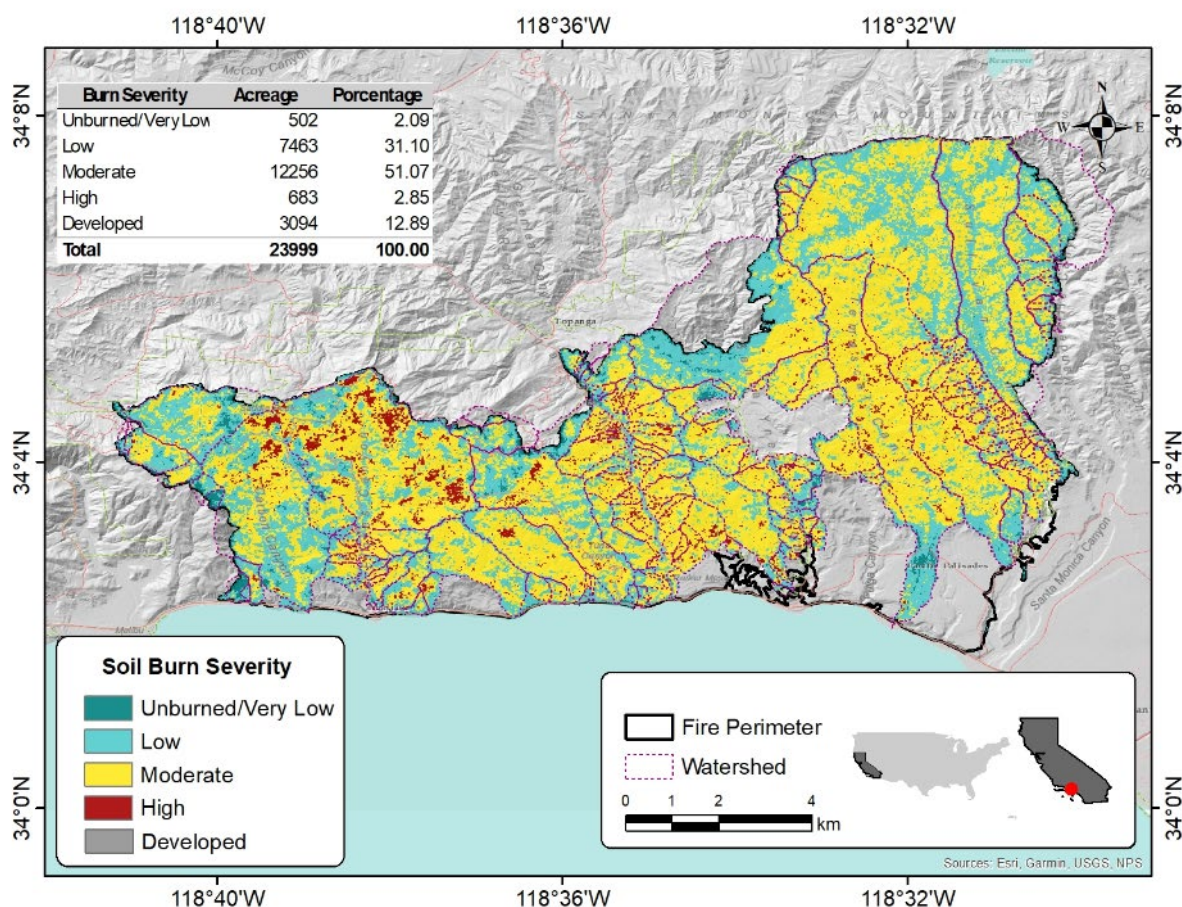
Burn Severity	Acreage	Porcentage
Unburned/Very Low	502	2.09
Low	7463	31.10
Moderate	12256	51.07
High	683	2.85
Developed	3094	12.89
Total	**23999**	**100.00**

Soil Burn Severity
- Unburned/Very Low
- Low
- Moderate
- High
- Developed

Fire Perimeter
Watershed

Sources: Esri, Garmin, USGS, NPS

Fig. 2.9. Soil burn severity map of the Palisades Fire burn area

In Mandeville Canyon, the slopes were composed of a residual sandy-silty soil layer, derived from a highly weathered and jointed massif of metamorphic rocks (slates), with variable depth ranging from 20 to 70 cm. Additionally, several colluvial deposits were present, with a composition that included gravel, sand, and clay. In Los Leones Canyon, on the north-facing slopes, surficial soils consist of an approximately 40-cm deep layer of sandy soil, overlying weathered sedimentary rock composed of conglomerate and sandstone. Surficial soils on the south facing slopes consist of clayey sand with gravel. Topanga Canyon is primarily underlain by Miocene sedimentary and volcanic units, specifically the Topanga Formation and Conejo Volcanics, which form ridges and

cliffs along the canyon walls. The surficial materials identified in Topanga Canyon consist of shallow sandy soils with variable amounts of silt and clay, colluvial-alluvial deposits, and weathered sedimentary rocks such as sandstones, siltstones, and conglomerates.

An ash layer was present at all the sites with varying thickness and continuity. On the February 4th visit in Mandeville Canyon, a thin (1 to 3 cm) layer of gray-white, black, and occasionally orange ash was covering the soil surface in the majority of the site (Fig. 2.10a). On the north-facing slopes of the Los Leones Canyon, the ash layer was less than 2 cm thick and discontinuous, whereas the thickness of the ash layer reached up to 10 cm on the south facing slopes (Fig. 2.10b). The ash layer was less widespread in subsequent field visits in February, March, and April but patches of ash were still present.

| (a) | (b) |

Fig. 2.10. Ash cover on February 4, 2025 in (a) Mandeville Canyon and (b) south-facing slopes of Los Leones Canyon (coordinates: 34.120333°, -118.506318°; 34.046944°, -118.559219°)

A quick water droplet test was used to qualitatively evaluate soil hydrophobicity in Mandeville Canyon on the February 4th visit. A water droplet was placed on the soil surface at various locations across the site and the infiltration was observed. Based on this test, some residual soils appeared to be hydrophobic, whereas the ash layers exhibited hydrophilic behavior. A mini disk infiltrometer test (Meter Group, Pullman, WA) was performed at two locations, one on soil and one on the ash layer. The saturated hydraulic conductivity was measured as 3.9×10^{-4} cm/s for the soil and 5.8×10^{-3} cm/s for the ash.

The burned vegetation was primarily mixed chaparral, typical of Mediterranean climate regions like the Palisades burn area, and other shrub and grass species including coastal scrub, and some valley oak woodland communities (CAL FIRE 2018). In the Santa Monica Mountains, the mixed

chaparral is composed of various large shrub species, including scrub oak (*Quercus berberidifolia*), greenbark or spiny ceanothus (*Ceanothus spinosus*), mountain mahogany (*Cercocarpus betuloides*), toyon (*Heteromeles arbutifolia*), hollyleaf redberry (*Rhamnus ilicifolia*), sugarbush (*Rhus ovata*), and manzanita (*Arctostaphylos spp.*) (NPS 2015). This plant community is widespread throughout California, covering much of the foothills and mountainous areas. It is a fire-adapted ecosystem, characterized by species with the ability to regenerate from seed after wildfires (NPS 2015). In the areas visited, these shrubs were deep-rooted and generally less than 4 m in height. The understory consisted of a layer of herbaceous vegetation (Fig. 2.11).
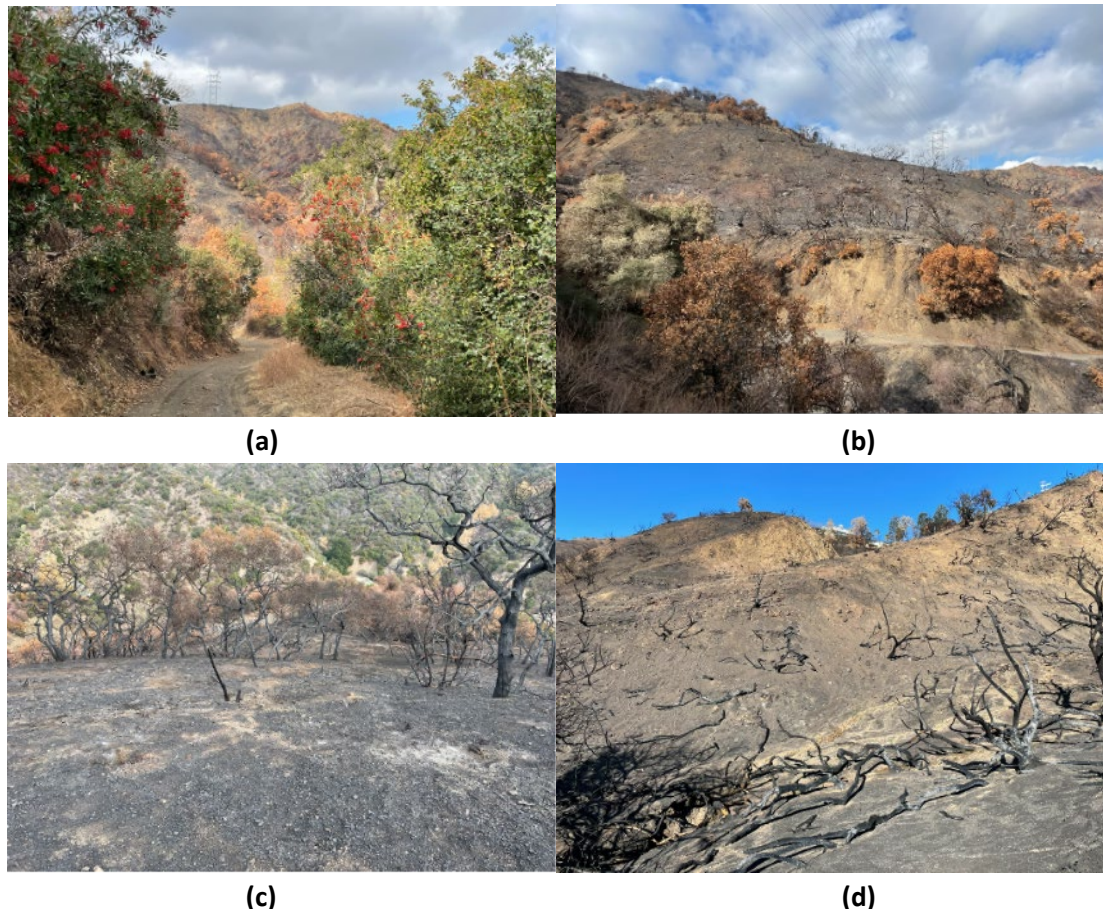

| (a) | (b) |
| (c) | (d) |

Fig. 2.11. Mixed chaparral, shrubs with different combustion completeness in a,b,c) Mandeville Canyon and d) Los Leones Canyon (coordinates: 34.120225°, -118.505867°; 34.118548°, -118.505496°; 34.118487°, -118.504911°; 34.047040°, -118.559080°).

Shrubs with varying levels of combustion completeness were observed throughout the burn area, some exhibited partially burned canopies but remained in place, while others were completely combusted and had collapsed, and in some cases were displaced downhill (Fig. 2.11).

Macropores were widespread at the slopes burned by the Palisade Fire, associated with the combustion of tree trunks and large roots (Fig. 2.12). Macropores can act as preferential pathways for water and ash and change the hydrology of the slopes (e.g., Akin and Akinleye 2021,

Akin et al. 2023). The diameters, shapes, and depths of the macropores varied, and in some cases, remnants of roots could still be identified within the macropores.

Fig. 2.12. Macropores due to combusted roots (coordinates: 34.120597°, -118.506639°; 34.117769°, -118.505200°; 34.046954°, -118.559453°)

2.6. Post-fire precipitation events

The area burned by the Palisades Fire has a Mediterranean climate with regional hydrology governed by rainfall. According to rainfall data from representative gauges in the burn area, or vicinity, the Palisades Fire was impacted by three significant storms starting with the first rainfall (approximately 27 mm) after the fire on January 25-26th, 2025 (Fig. 2.13). The subsequent rain events in February were larger and increased the cumulative precipitation to 200 mm.
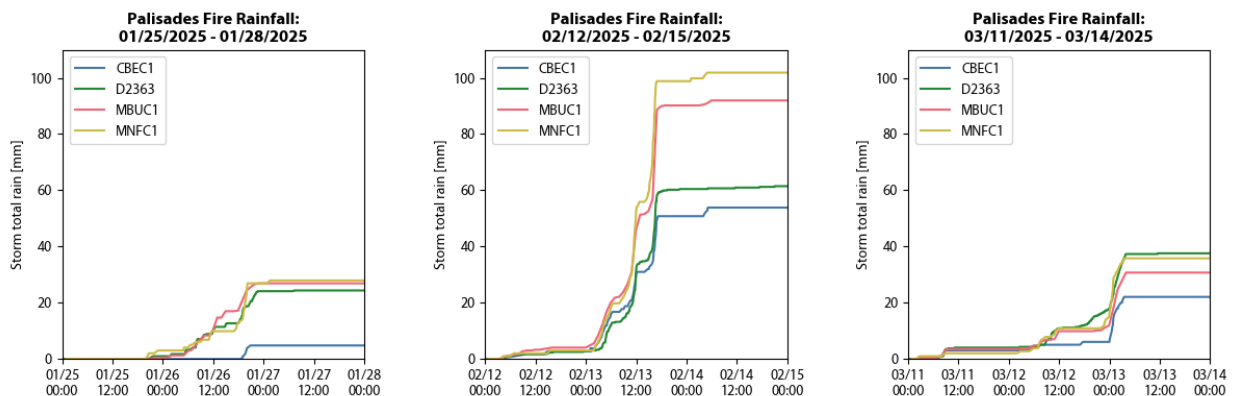

Fig. 2.13. Rainfall accumulation data for three storms impacting the Palisades Fire. See Fig 1.4 for gauge location.

Rainfall data shown in Figure 2.14 were obtained from Synoptic Data using the Weather API (Synoptic 2025) and from the Weather Underground Wundermap application (Wunderground 2025). The 15-min and 60-min peak rainfall intensity data during the January 25th, February 13th, and March 13th storms were gathered from each of these gauges. The 15-min peak rainfall intensity reached 64 mm/h during the February 13th storm.
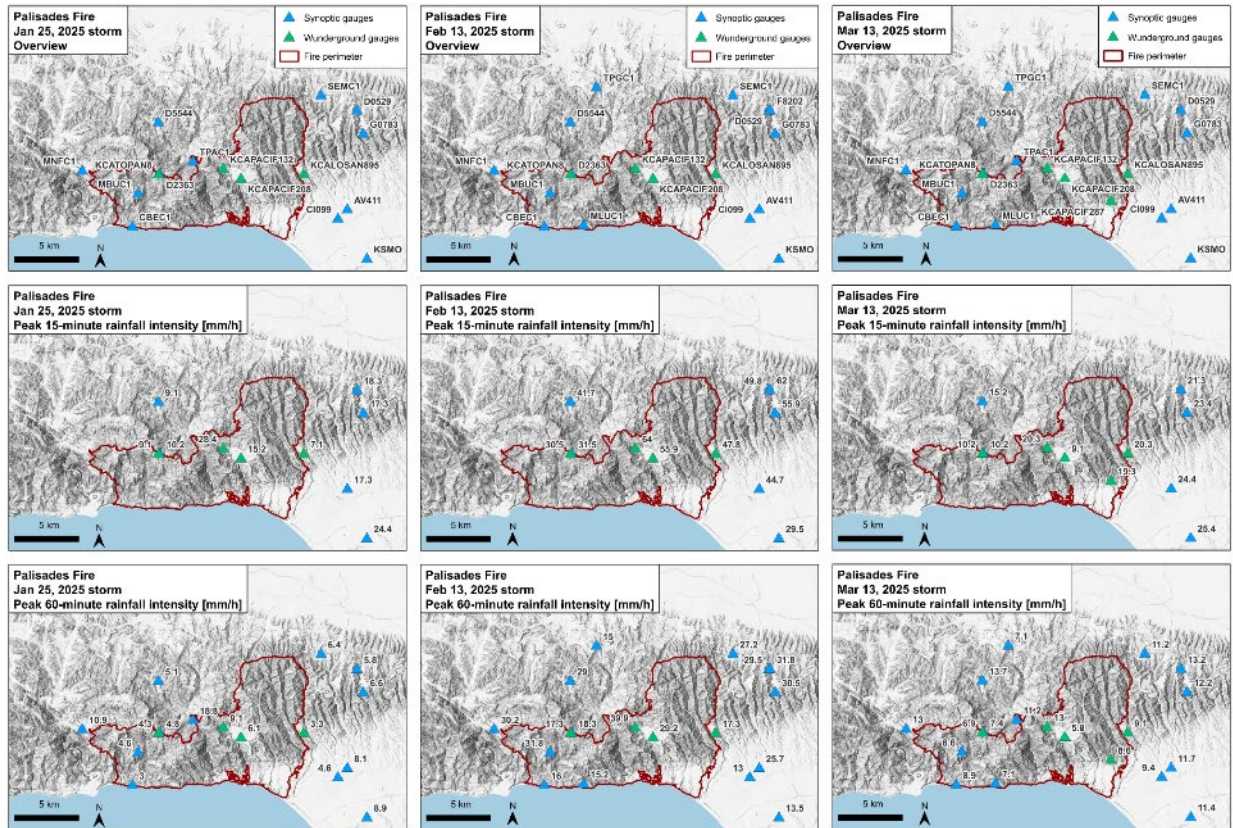
Fig. 2.14. Rainfall distribution across the Palisades for three storm events.

2.7. Erosion, Debris Flows, and Landslides

2.7.1. Erosion

Signs of erosion, particularly in the form of dry ravel and rill erosion, were widespread within the fire perimeter. Extensive rills were documented in all the canyons that were visited. The rills that were documented in Mandeville Canyon after the January storm progressed into gullies after the February storm (Fig 2.15). Similar extensive rilling and progression to gullies were observed in Topanga and Los Leones Canyons.
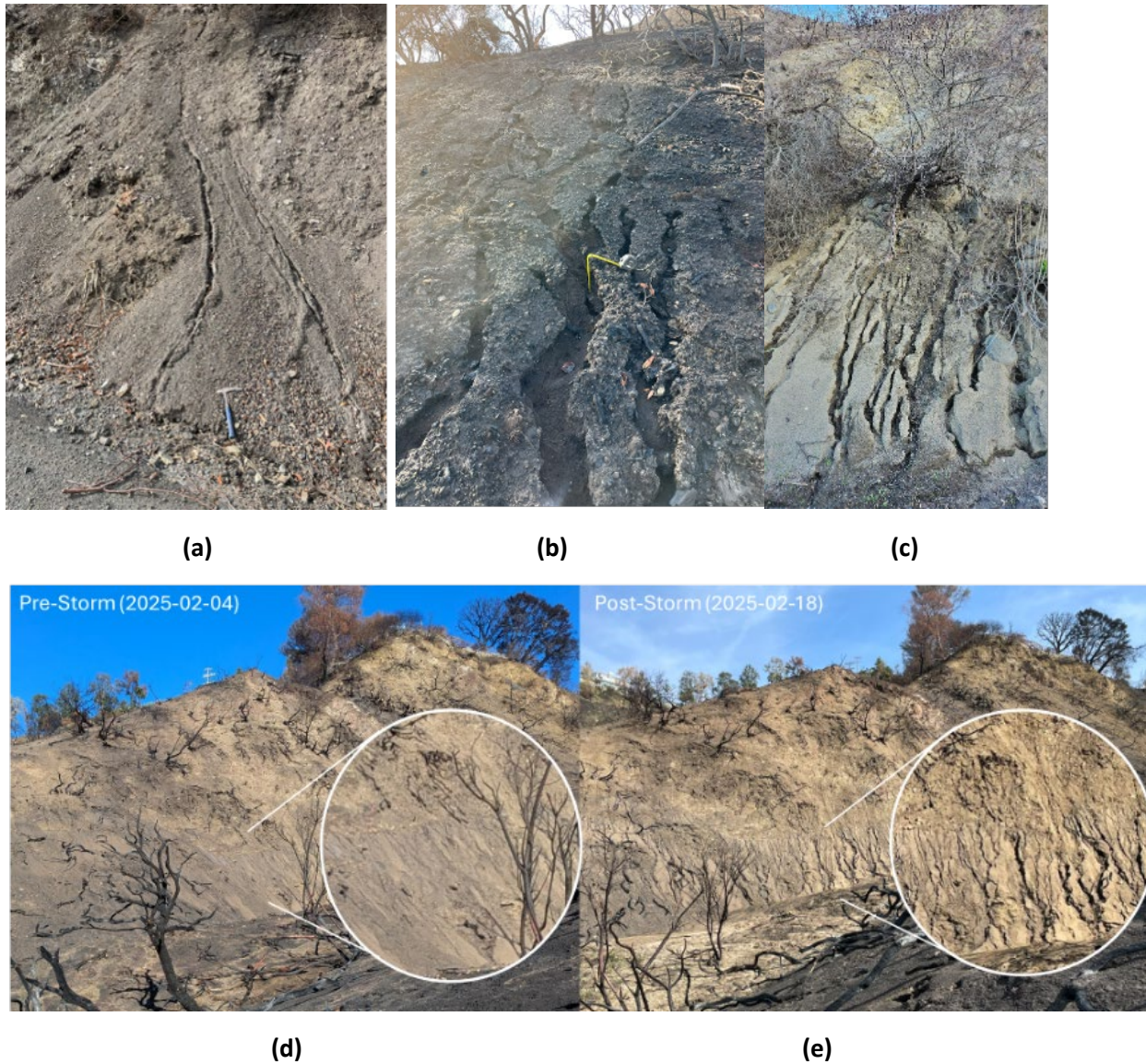
Fig. 2.15. Rills after the (a) January storm in Mandeville Canyon, (b) after the February storm in Mandeville Canyon (c) after the February storm in Topanga Canyon, and (d) before and (e) after the February storm on north-facing slopes of the Los Leones Canyon (coordinates: 34.117472, -118.505577; 34.118487, -118.504911; 34.062801, -118.587177; 34.047316, -118.559135)

2.7.2. Debris Flows/Debris Floods

Postfire runoff response from the January 25 and February 13 storms was documented through personal accounts, reports by colleagues, and media reports. The types of runoff response, ranging from flood flow to debris flow, and their spatial distribution, are shown for the Palisades fire in Fig. 2.16. No post-storm runoff responses were reported following the March 13, 2025 storm.
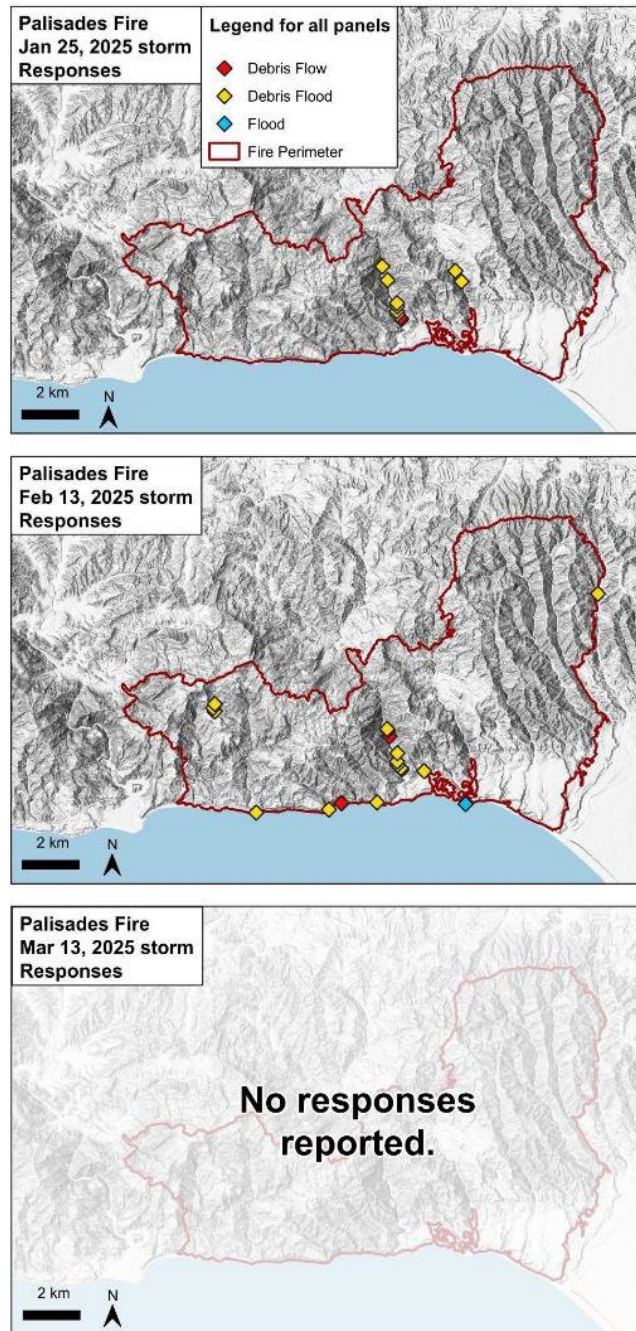
Fig. 2.16. Observed flow responses at the Palisades Fire for the January 25, February 13, and March 13 storms. Points are colored by flow type and located at the basin outlet where the observation was made.

Postfire flow types occur on a continuum ranging from flood flows to hyperconcentrated, or sediment- and debris-floods, to debris flows. The distinction between flows along this continuum is made based on the volumetric sediment concentration and grain size distribution.

Characteristics differentiating flood flows, debris floods and debris flows are adapted from Hungr et al. (2001) and Pierson (2005a,b) as follows:

Flood flows – closely resemble normal streamflow with sediment concentrations less than 20% by volume, bedload transport composed of sands to cobbles, and have predictable Newtonian fluid behavior

Debris floods – rapid, surging flow that is heavily charged with debris and sediment. Suspended sediment composed of sand-sized particles is common with bedload transport composed of cobbles to boulders. Approximately Newtonian flow behavior with 20% to 60% sediment concentration by volume. Transient debris dams of boulders and woody material are common. Highly erosive.

Debris flows – rapid, surging flow composed of a slurry of sediment and water with suspended gravels and boulders. Less predictable non-Newtonian flow behavior with sediment concentrations of > 50% by volume. Has the ability to cause catastrophic damage from burial and impact that can infill and divert streams, and destroy automobiles, buildings, and infrastructure.

Evidence of debris floods and flows was observed near Topanga Canyon Road. A site visit immediately following the February 13th storm revealed significant sediment deposition and road blockages along State Route 27. Debris flood deposits from a small, steep tributary to the east were observed. These deposits consisted primarily of woody debris, boulders (ranging from ~0.1 m to > 0.5 m), cobbles, and fine-grained sediments (Fig. 2.17). Several sections of the road were covered by floodwaters, mudflows, debris, and sediment transported from tributaries and adjacent hillslopes (Fig. 2.18). Increased sediment accumulation was also observed within the channel of Topanga Creek (Fig. 2.19). A postfire debris flow that was triggered during the January 26, 2025 storm event was documented by Caltrans (Fig. 2.20). The extent of debris floods and flows following the January 25-26 and February 13 storms was significantly greater than under pre-fire conditions (personal communication, Caltrans).

Fig. 2.17. Debris flood deposits near State Route 27 in Topanga Canyon. Damaged roadside rails resulted from flow impacts. The exposed deposit wall reveals stratification in flow near the surface (coordinates: 34.070734°, -118.588038°).

Fig. 2.18. Fine-grained sediments and rock debris from flood/flows accumulated near post mile 1.8 on State Route 27, where a landslide occurred in 2024. Metal mesh walls were damaged, and large boulders were transported downslope from steep terrain, with some remaining unstably positioned on the slope (coordinates: 34.063016°, -118.585803°).

Fig. 2.19. Drone optical image comparison before and after the Feb 13 storm. The debris flood/flow deposits near the State Route 27 road are shown in Figure 2.17.

Fig. 2.20. Postfire debris flow triggered during the January 26, 2025 storm and was composed of a slurry of mostly fine-grained sediment. Source: Caltrans (34.05035°, -118.58025°).

2.7.3. Landslides

Reconnaissance was performed in the Castellammare area with a focus on areas of prior landslides. There are many remedial landslide measures that have been installed in the area over the last ~75 years, including soldier pile retaining walls. Several of the soldier pile retaining walls had timber lagging, which had partially burned during the Palisades Fire. Many of the houses in the burn area of Castellammare were destroyed by fire, while others survived.

The Castellammare area is within the Pacific Palisades district of the City of Los Angeles, California. This area is within the Santa Monica Mountains and the mountainous area immediately adjacent to the coastline. Pacific Coast Highway is at the base of the slopes of Castellammare, and the slopes have many residential streets and single-family residences. Pacific Coast Highway was graded in 1922 and included cutting into the toe of the slopes of Castellammare. In 1925 and 1926, the development of Castellammare occurred, with construction of residential streets, water mains, storm drains, and sanitary sewers. As part of the grading, some retaining walls were also constructed. In 1932 through 1935, further widening of Pacific Coast Highway occurred, with further cuts into the toes of the slopes. Beginning in 1932, slope movement was observed, with some minor slope stabilization measures taken. The slopes began causing severe damage to infrastructure in 1935. By 1958, a number of houses had been rendered un-occupiable by slope movements. Several streets were cut off in subsequent landslide movements. In 2010, URS did an evaluation of the Tramonto landslide, a major landslide within Castellammare, including potential mitigation strategies (URS 2010). A geologic cross section and a geologic map of the area are illustrated in Figs. 2.21 and 2.22.

Fig. 2.21. Geologic Cross-Section through Tramonto Landslide in Castellammare (URS 2010).
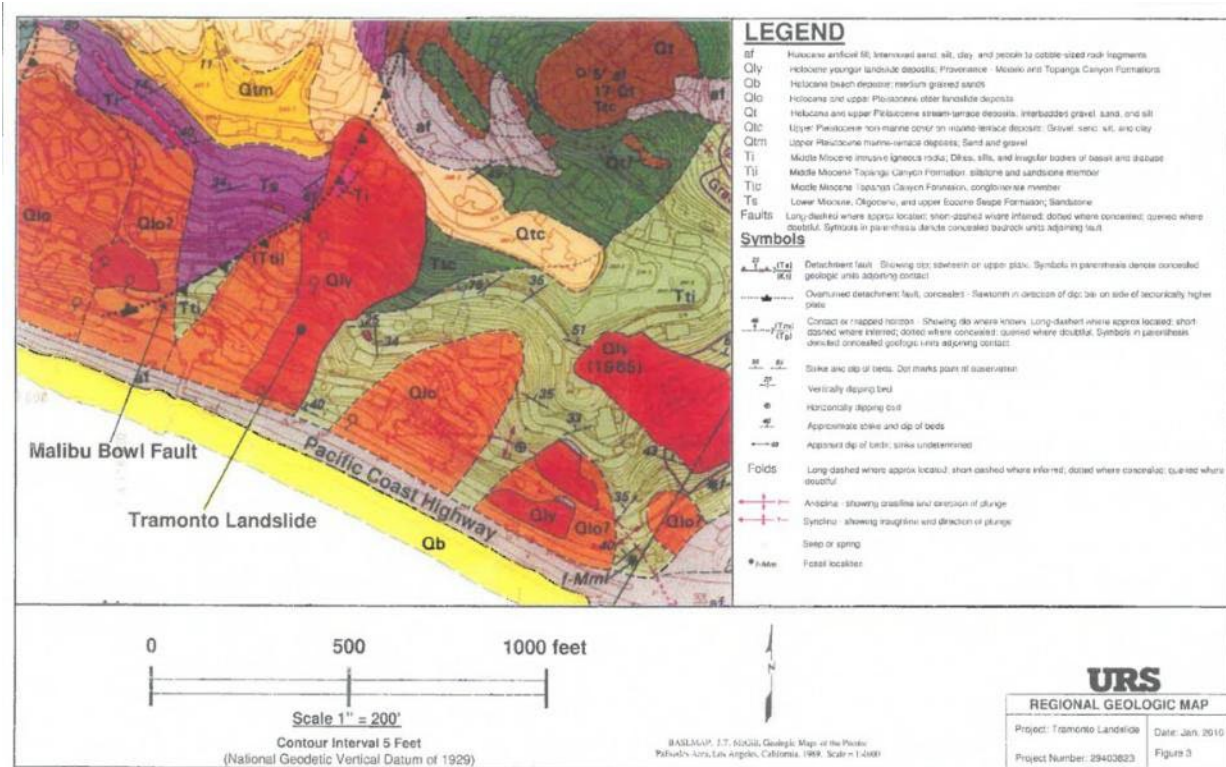
Fig. 2.22. Geologic map of Castellammare area (within the burn zone, URS 2010)

A significant landslide occurred following the Palisades Fire in Castellammare between Castellammare Drive and Posetano Road at the location shown on Fig. 2.23. Houses near the top of the landslide burned, above-ground storm drainpipes upstream of the landslide burned and were no longer functioning properly, and after a few days, the landslide occurred, destroying a house at the base of the landslide, as shown in Fig. 2.24. Further intrusion of water due to broken water supply pipes (per communication with local residents), and storm water flow pattern changes due to burned storm drain pipes uphill of the areas (on Revello Dr.) as shown on Figures 2.25 and 2.26, may have contributed to an increase of water in the slope. A resident of the area (Ms. Elaine Culotti) reported in the rainfall event that followed a few days after the Palisades fire, that water was flowing from the location of the burned storm drainpipe toward the crest of the slope on Revello Dr. as shown in Figure 2.26. As another example of post-wildfire storm water diversion due to burned storm drains, another location on Revello Dr. (east of the landslide) was also exposed to increased storm water due to another burned pipe as illustrated in Fig. 2.27.

It appears that land movement in this area preceded the fire. A Google Earth image from August 2022 shows a failing retaining wall at rear of the house with several drainpipes draped over the wall (Fig. 2.28). The concrete wall appears to be rotated outward with open fractures showing offset.

34

Fig. 2.23. Location of the 2025 landslide in Castellammare (From Google Earth).

Fig. 2.24. House damaged at toe of the 2025 landslide, Castellammare Dr., Pacific Palisades (2/4/25).

Fig. 2.25. Storm drainpipe completely burned on Revello Dr., upslope of the 2025 Castellammare landslide (4/1/25).

Fig. 2.26. Burned storm drainpipe in relation to the 2025 Castellammare landslide (4/1/25).

Fig. 2.27. Storm water diverted to descending slope due to burned storm drainpipe (photograph from video courtesy of Elaine Culotti) (coordinates 34.04041667°, -118.5567167°).

Fig. 2.28. Google Earth image from 8/22, showing a failing retaining wall at rear of the house with several drainpipes draped over the wall.

A potentially unstable area that exhibited visible cracks was observed (Fig. 2.29) in Mandeville Canyon. The tension cracks were above a roadway cut. This area will be monitored after future rain events for potential landslides.

Fig. 2.29. Tension cracks above a roadway cut in Mandeville Canyon (coordinates: 34.116578°, -118.505380°).

At postmile 1.8 along State Route 27 (Topanga Canyon Boulevard), a north-south roadway through Topanga Canyon, a hillside near an S-curve has experienced several episodes of major landslides (Figure 2.30). The first occurred in 1940 and is located on the northwest side of the hillside. The second and most recent event, on March 9, 2024 (Caltrans 2024), is located on the southeast side of the slope. Both landslides exhibit distinguishable scarps and planar failure surfaces, suggesting translational slides affecting hillside debris associated with colluvial deposits overlying sandstones and conglomerates of the Tuna Canyon Formation.

Using two Digital Elevation Models (DEMs) surveyed before (2015) and after the fire (January 2025), with a spatial resolution of 1 m per pixel (OpenTopography Dataspace - Topographic differencing spanning the 2025 Palisades and Eaton Fires, LA), Brigham et al. (2025) calculated a differential Digital Elevation Model (dDEM) (Figure 2.31). The resulting dDEM highlights areas with decreased elevation caused by erosion (red), and the ravel sediment deposits (blue). The 2024 Topanga landslide and subsequent removal of landslide debris is visible on the eastern side of the canyon.

Fig. 2.30. Topanga Canyon landslides. (a) Google Earth image of the S-curve on State Route 27; (b) Drone photo of the area taken on 3/24/25, courtesy of Syrusa Engineering (coordinates: 34.063365°, -118.586363°).
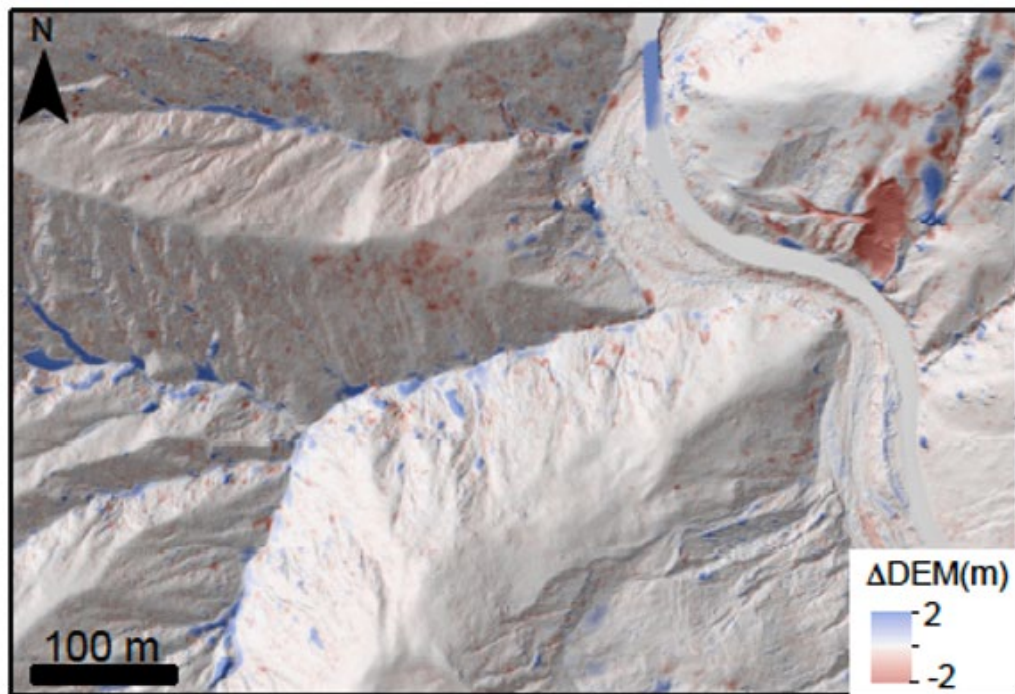

Fig. 2.31. Digital elevation map differences (dDEM) in Topanga Canyon from airborne lidar DEM difference from 2015 to 2025, before and after the Palisade Fire Brigham et al. (2025).

After the storm on February 13th, the area showed more sediment movement, marked by debris and mud blocking the roadway (Fig. 2.32). During the field visit on March 24th, debris was observed covering the ash layer associated with the 2025 wildfire in the area of the 1940 landslide scarp. This area is expected to continue experiencing slope instabilities in the form of erosion, debris flows, and landslides in response to continued rainfall and the presence of uncemented surface materials, including colluvium and man-made deposits at the base of the slope, and therefore will be included in the team's long term monitoring plan.

(a)   (b)

Fig. 2.32. (a) Mud and debris blocking State Route 27 after the February 13, 2025 storm. (b) Debris covering the ash layer in the 1940 landslide area (coordinates: 34.063016°, -118.585803°; 34.063365°, -118.586363°).

2.8. Debris Retention Structures

A debris retention structure was observed in Mandeville Canyon before and after the two February storms (Fig. 2.33). The retention structure was constructed across a drainage swale. Some soil and organics were retained in the basin before the February storm. After the storm, the retained sediment thickness increased by 0.5 to 1.2 m. The structure showed signs of deformation and distress relative to its state before the February storm. The structure has approximately another 0.5 to 1 m of height of debris it can retain before overtopping.

A traditional debris retention structure constructed with timber materials was observed in the Mandeville Canyon before the January storm (Fig. 2.34). The structure was partially burned.

(a)	**(b)**

Fig. 2.33. Photographs of debris retention structure (34.120097°, -118.506599°) in Mandeville Canyon (a) before the major rainfall events taken on 2/4/25 and (b) taken on 2/18/25, after significant rainfall events.

Fig. 2.34. Photograph of a partially burned debris retention structure (34.1061, -118.50564) in Mandeville Canyon before the January storm.

2.9. Damage to Infrastructure Systems

2.9.1. Water

Elements of the potable water supply systems in the Palisades Burn area were observed on February 4, 2025, which was 28 days after the start of the fire event. These fall within the jurisdiction of the Los Angeles Department of Water and Power (LADWP) and the Los Angeles County Public Works. The following were specifically visited: pump stations, above-ground water supply pipelines, and a circular tank water reservoir. A water retaining dam was observed from a

distance. The at distribution systems were reportedly contaminated and issued 'do not drink' orders shortly after the fires, as evidenced by public notice signage posted around the burn areas. On February 4, 2025 the area supplied by LA County Public Works had removed the 'do not drink' order and were delivering potable water to customs through the network. Whereas, the 'do not drink' order remained within the burn area served by the LADWP.

Water pipelines made of iron and mechanical joints were constructed at grade in the Big Rock Mesa region operated by LA County, likely because the area is prone to slope movement. The above-ground pipelines did not appear to have been damaged severely by the fire. An example is shown in Figure 2.35. Other pipelines in the area were clearly in operation on February 4, 2025 when observed.

Fig. 2.35. Photograph of above-ground water supply pipeline with slope-movement mitigation expansion joints (34.0412773°, -118.6194627°) in Big Rock Mesa area.

The Temescal Tank is owned and operated by the LADWP and located at the highest elevation over the Palisades Highlands area and within the burn zone. The partially buried concrete tank is shown in Fig. 2.36. Visually, signs of large-scale damage to the tank were not observed, but from the appearance of partially scorched and some new ancillary equipment and recent grading/erosion control work using jute mesh at the circular tank, it appeared some fire damage may have occurred to some of the equipment associated with the water tank. The new equipment had apparently been repaired prior to our visit.

Fig. 2.37 illustrates the LADWP Trailer Pump Station in the Palisades Highlands area that survived the fire whereas many structures in the area had burned down. This pump station lifts potable water up to the Temescal Tank from a buried tank immediately next to it that seemingly was not physically impacted by the fire due to its soil cover. The Santa Ynez Pumping Station is also

located in the Palisades Highlands area about a mile from the Trailer Pump Station and also was not damaged by the fire even though other surrounding and nearby structures were. The Santa Ynez Pumping Station is located below the Santa Ynez Reservoir that was reported to be out of service (i.e., not containing any water) at the time of fire due to work needed on its floating cover. Fig. 2.38 shows the downstream slope of the Santa Ynez Reservoir Dam lined with rows of straw wattle to prevent erosion of the compacted earth embankment after its natural ground cover was burned.

Fig. 2.36. Photographs of the Temescal Tank circular water supply tank in Palisades Highland. Recent slope erosion mitigation (with jute mesh) had been performed behind the tank (likely post-fire), and some of the ancillary equipment attached to the tank may have been recently repaired based on observations, some equipment was scorched by the fire. (34.0777306°, -118.546853°).

Fig. 2.37. Photograph of the LADWP Trailer Pump Station in Palisades Highlands (architecturally disguised to appear similar to residential structures) in the burn area. Many burned houses were in the vicinity of the pump station (34.07438131°, -118.550311°).

Fig. 2.38. Photograph of the LADWP Santa Ynez Reservoir Dam in Palisades Highlands in the burn area showing straw wattle to protect against future erosion of the compacted earth embankment after the fire burned the natural ground cover (34.073142°, -118.569466°).

2.9.2. Wastewater

The field reconnaissance team sought specific locations of sanitary sewer wastewater infrastructure performance within the Palisades region. There were no findings of impacts to the wastewater system at the time of this report. However, as shown in Fig. 2.39 there were many observations of portable toilets at residential and commercial buildings in the Palisades area that were located for purposes other than for construction and repair crews (i.e., in driveways and side yards of homes and businesses). Since the wastewater system is on hillsides, it is expected to be a full gravity flow system and therefore the need for portable toilets is curious and implies some level of impact to the wastewater system from the fire. Future reporting will attempt to include potential impacts to wastewater.

Fig. 2.39. Portable toilets in the Palisades residential neighborhood. Many homes and businesses that survived the fire were observed to be using portable toilets on 2/4/25.

2.9.3. Storm Drains

Storm drain pipes were exposed at the ground surface at a number of locations we observed, as they had been placed in areas of prior landsliding and had been constructed (temporarily) in a manner that could be maintained after future landslide movements. An example is shown in Fig. 2.40. These surface-exposed storm drain pipes had significant damage, at joints (as shown in Fig. 2.40), or had completely burned away/melted. The storm drain shown in Fig. 2.40 collects surface water flowing from above canyons at a large catch basin located on the streets above. The pipeline normally routes the runoff water around the homes located below (i.e., to the left of photos in Fig. 2.40); in the absence of the drainage pipe the neighborhood is exposed to threat of flood.

(a)	**(b)**

Fig. 2.40. Storm drain pipe damaged by Palisades Fire. Between Big Rock Dr. and Seaboard Rd, Big Rock Mesa, Malibu, CA (2/4/25).

After the fire the drainage basins and surface runoff were protected with waddle as shown in Fig. 2.41 to reduce the spread of contaminants.

Fig. 2.41. Surface runoff and storm drain basins protected against spread of contaminants (2/4/25).

2.9.4. Natural Gas

The field reconnaissance team sought specific locations of natural gas infrastructure performance within the Palisades region. There were no findings of impacts to larger components at the time of this report, like those reported for water systems, however there were findings of impacts

within the natural gas distribution system. Fig. 42 shows a natural gas meter on a property where a residential home had burned.

Fig. 2.42. Natural gas meter at burned residence (2/4/25).

It was common for the gas meters to burn with the homes, along with the gas line shutoff valve that is located at the meter. The burned lines resulted in a free-flow of natural gas from the service line pipes in locations where the distribution system could not be shut down in advance, which became another source of ignition. In neighborhoods where some homes survived the fires, those that burned were found to have a small steel trench plate in the street in front of the property, which is interpreted to be the location where the gas company made a small excavation to access the service line to install a new shutoff valve allowing the distribution line to continue servicing the surviving homes.

2.9.5. Electric Power

A large steel truss tower supporting high-voltage transmission lines was observed at the top of a ridge in the burn area adjacent to Mandeville Canyon (location: 34.117998°, -118.505385°, Fig. 2.43). The fire had clearly burned around the entire base of the tower and had burned hot enough to melt a fire camera station approximately 5 m west of the tower, but there were no signs of fire-related damage to the steel tower or the tower's concrete foundations. To the north and south of the tower there are steep slopes. The slope on the north side is larger and has a height of 43 m over a horizontal distance of 54 m from the base of the tower to the fire road near the bottom of the slope. The existing slope stabilization measures consist of rock nets, steel cables,

and fences to catch falling debris. All the stabilization measures appear to only be intended for mitigation of surficial instabilities.
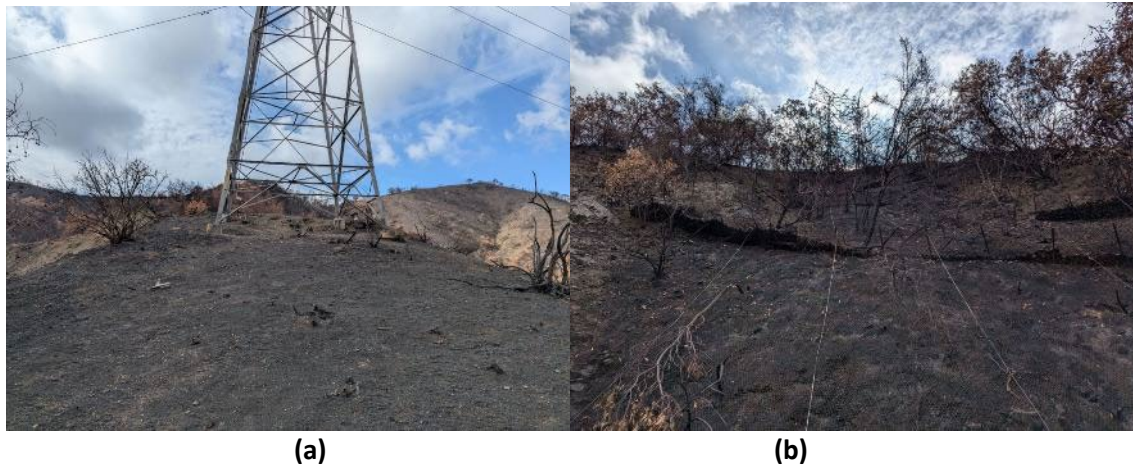

<div align="center">(a)   (b)</div>

Figure 2.43. High-voltage transmission tower in the burn area adjacent to Mandeville Canyon before major rainfall (2/4/25). (a) Photograph viewing the base of the tower (b) Photograph viewing steep slope with engineered slope-stability mitigations directly beneath the tower (coordinates: 34.118310°, -118.505174°, 34.118533°, -118.505498°).

The tower and north slope were observed again after the major rainfall events. A team of laborers were transporting sandbags to this slope where they were being placed along the edge of the fire road (Fig. 2.44).

Fig. 2.44. View of fire road below the slope immediately north of the high-voltage tower adjacent to Mandeville Canyon after the major rainfall (coordinates: 34.118533°, -118.505498°).

The slope did not appear to have any global instability before or after the rainfall and there was no significant surficial movement other than some rilling (Fig 2.45).

(a)   (b)

Fig. 2.45. View of the slope immediately north of the high-voltage tower adjacent to Mandeville Canyon (a) before major rainfall (2/4/25) (b) and after major rainfall (2/18/25) (coordinates: 34.118533°, -118.505498°).

Fig. 2.46 shows the repair of electric power distribution line poles along the Pacific Coast Highway. The replacement poles were made of steel material. Many of the poles existing before the fire were wooden. Many buildings that survived the fire were using mobile electric power generators to power the homes and businesses.
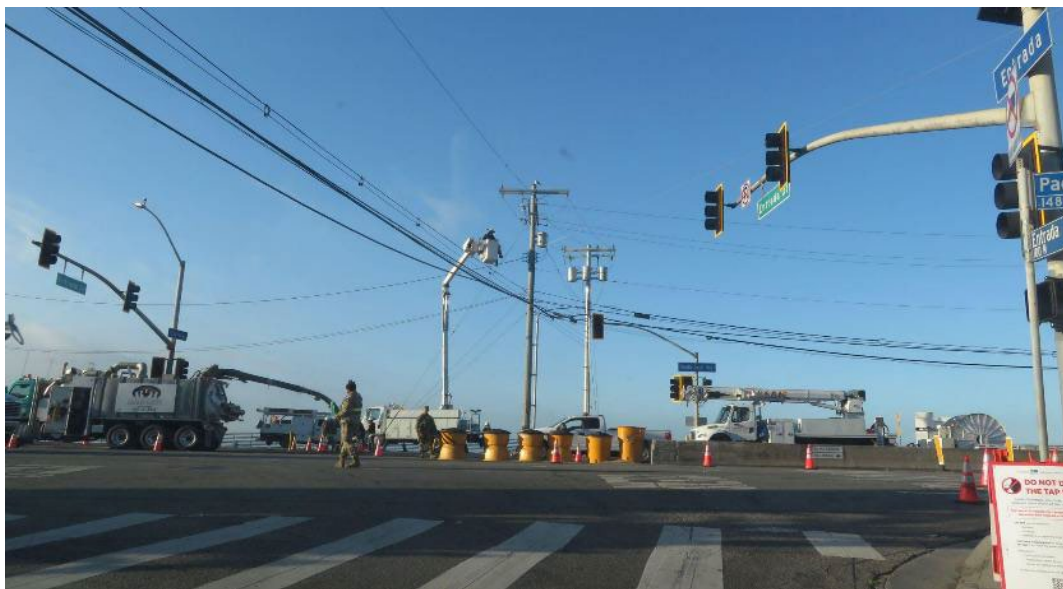

Fig. 2.46. Repair of electric power distribution lines replacing burned wooden poles with steel poles (2/4/25).

2.9.6. Telecommunications

The field reconnaissance team sought specific locations of telecommunications infrastructure performance within the Palisades region. There were no findings of impacts to larger components at the time of this report, however, there are known telecommunications facilities along the ridges of the mountains in the area that are highly susceptible to impacts from the fire. Future reporting will attempt to include potential impacts to telecommunications facilities. Fig. 2.47 shows mobile cell units located along the Pacific Coast Highway. It is unknown if these were to replace damaged cell sites or for specific emergency communication purposes.
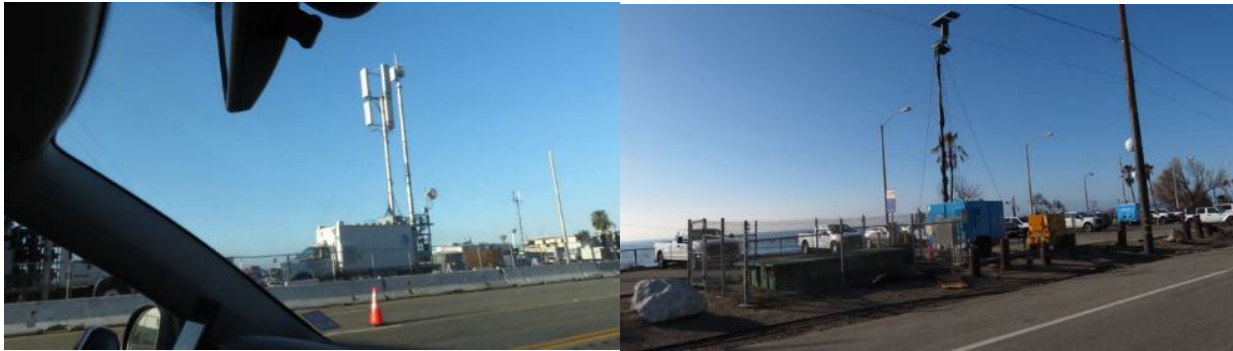

Fig. 2.47. Mobile cellular communications units placed along Pacific Coast Highway (2/4/25).

2.9.7. Pavements and Roadside Infrastructure

Roadways showed multiple signs of heat-related damage and obstruction due to fire debris. In Fig. 2.48a, burned vegetation lines both sides of the street, with ash and charred remnants accumulating along the curbs and gutters. Portions of the asphalt appear darkened or surface-seared, and debris from burned structures—such as melted plastic, cables, and fencing—has encroached onto the roadway. In Fig. 2.48b, the intersection area shows scorched curbs and bollards, and soil displacement near roadside signage and utility poles. The crosswalk area appears intact, but surrounding infrastructure is visibly affected by heat and soot deposits. In Fig. 2.48c, collapsed brick walls and melted fencing materials have fallen into the driving lane. The asphalt adjacent to these debris piles shows visual signs of charring and fine particulate accumulation. Overhead utility lines and poles remain upright, but the sidewalk and shoulder areas are extensively burned.

After the fire, several roadways were protected against erosion and debris running onto the drive surface by using k-rails as shown in Fig. 2.49.

-118.546909°   34.0452948°   3514800   MARQUEZ AV

(a)

-118.5467813°   34.0463287°   3514800   MARQUEZ AV

(b)

-118.5488324° 34.0439833°   3514900   MARQUEZ AV

(c)

Fig. 2.48. Damage to pavements and roadside infrastructure in Pacific Palisades. (a) Vegetation and structural debris burned along the road edge, with heat-induced discoloration and material accumulation on the asphalt. (b) Scorched bollards, sidewalk curbs, and fire-related surface disruption near pedestrian and traffic signage infrastructure. (c) Collapsed brick fencing and warped plastic materials spilling onto the pavement, with surrounding areas of the road and sidewalk visibly charred.

Fig. 2.49. K-rail installed along roadways in the Palisades and Malibu areas soon after the fire to protect the drive surface from debris, erosion, and runoff.

2.9.8. Retaining Structures

Some slope areas with prior surficial instability had slope netting to reduce rockfall hazard; such rock netting in the areas observed showed signs of burning (discoloration), but appeared to be intact (although the potential weakening of the netting is not known), as shown in Fig. 2.50.

Fig. 2.50. Rock netting with discoloration indicating fire exposure in Palisades Fire. Big Rock Dr., Malibu (2/4/25).

Soldier beam and tie-back anchor retaining walls have been installed in the last 50+ years in Pacific Palisades to assist in stabilization of roadways, where landslides have caused significant road damage/movement. These retaining walls, although permanent, often used treated timber lagging between soldier piles. An example of a tied-back soldier pile wall at the Tramanto Landslide that has partial shotcrete lagging and partial timber lagging is shown in Fig. 2.51. At this location, although the fires passed through this area (most of the houses on both sides of the street at this location burned down), the timber lagging was largely intact (but the degree of damage to the strength of the lagging or exposed steel soldier piles is not known). Fig. 2.52 shows one of several soldier beam with timber lagging tie-back walls along the Pacific Coast Highway. In some cases the timber lagging was burned as shown in Fig. 2.52 to 2.55. The integrity of the walls and tie-backs seem to remain intact.

Fig. 2.51. Soldier beam and tie-back anchor retaining structure with combination of timber and shotcrete lagging. Upper edge of Tramanto Dr. Landslide, Tramanto Dr., Castellammare, Pacific Palisades (2/4/25).

Fig. 2.52. Soldier pile with timber lagging retaining wall with tie-backs along Pacific Coast Highway. The timber lagging was burned in some locations (2/4/25).

Fig. 2.53. Image of soldier pile wall with damaged timber lagging that retains soil along outside edge of road prism (34.059966°, -118.637916°).

Fig. 2.54. Image of soldier pile wall with damaged timber lagging that retains soil along outside edge of building pad that supports foundation of a burned structure (34.0408°, -118.64546°).

Fig. 2.55. Images of wood lagging completely burned out. The wood lagging supported slopes at several locations along the Pacific Coast Highway prior to the fire (2/4/25).

Crib wall retaining structures with fire damage were observed (Fig. 56). The wall face showed burn marks, and the pre-fire vegetation growing out of the wall face was combusted, but otherwise no evidence of wall damage or instability was observed.

(a)

(b)

(c)

Fig. 2.56. Crib Wall with Burned Surficial Vegetation and Fire Exposure in Palisades Fire. (a) Post-Fire, (b) Pre-Fire Google Street View Image, (c) Close-Up of Burned Surface. Calle Patricia at Calle Jermaine, Palisades Highlands, Pacific Palisades (a and c taken 2/4/25).

Fire damage was also observed in stucco-faced short masonry retaining walls (Fig. 2.57), which remained intact.

-118.53877°   34.0520076°   3117100   LAS PULGAS RD

Fig. 2.57. Stucco-faced short retaining wall remains intact, with debris accumulation above the slope.

Shotcrete-treated slopes along the Pacific Coast Highway showed some burn marks but appeared to be undamaged (Fig. 2.58).

-118.5629706° 34.0409637°   4171100   PACIFIC COAST HY

Fig. 2.58. Shotcrete-treated slopes along the Pacific Coast Highway remained largely undamaged.

Soldier piles and wood lagging were also used as rockfall barriers along the Pacific Coast Highway in the Malibu area. Fig. 2.59 shows a set of soldier piles that supported wood lagging prior to the

fire. The lagging burned and was replaced with chain link fencing soon after the fire to protect the highway.

Fig. 2.59. Soldier pile and wood lagging rock barrier wall along the Pacific Coast Highway in Malibu area. The wood lagging completely burned out and was replaced with chain link fencing soon after the fire. The photo on right shows remaining evidence of the burned out wood lagging (February 4, 2025).

2.9.9. Structural Damage

The aim of the present investigations was not to document the performance of building structures such as houses. As described in Section 1.2, GEER personnel were aware that other reconnaissance teams were focusing on such data collection, which will also be aided by the extensive post-event imagery described in Sections 1.2 and 1.3. Nonetheless, GEER's personnel were in the field in areas with many burned structures, and here we record representative observations.

Widespread destruction to both coastal and hillside structures was observed. In several locations, most combustible materials—including wood framing, insulation, roofing, and interior contents—were completely consumed. In Fig. 2.60a, a coastal structure along the Pacific Coast Highway has been reduced to its steel frame, while nearby slope-side infrastructure, such as utility poles, also shows signs of damage. Debris from the burned structure and adjacent hillside is scattered near the road, where barriers have been placed. Fig. 2.60b shows another structure with only a steel skeleton remaining—no cladding or roofing remains, and the frame exhibits signs of heat deformation, indicating prolonged exposure to intense fire. In Fig. 2.60c, remnants of multiple residential buildings show only vertical masonry elements such as chimneys and partial wall sections still standing, highlighting the vulnerability of timber-framed construction in high-intensity wildfire zones.

-118.595204°   34.0399712°   4790400   SANDY CAPE DR

(a)

-118.5493906° 34.041858°   3515200   MARQUEZ PL

(b)

-118.5565574° 34.074359°   4181100   PALISADES DR

(c)

Fig. 2.60: Structural damage in Pacific Palisades. a) Coastal structure along Pacific Coast Highway reduced to a steel frame, with nearby utility infrastructure impacted and debris scattered near the slope. (b) Freestanding steel skeleton remains of a building, with all combustible materials consumed by intense fire. (c) Burned residential neighborhood showing only masonry chimneys and partial walls left standing amidst widespread structural loss.

2.10. Field Instrumentation and Long-Term Monitoring

The GEER team installed field instrumentation including soil water potential and water content sensors to monitor the long-term changes in soil water retention, rain gauges to monitor the precipitation, and debris flow monitoring stations. Part of the instrumentation is complete and part is ongoing. Fig. 1.4 shows the instrumentation locations.

Soil water potential sensors (TEROS 21, Meter Group, Pullman WA) and soil water content sensors (TEROS 11, Meter Group, Pullman, WA) were installed in Mandeville, Topanga, and Los Leones Canyons at three different depths (0.1 m, 0.3 m, and 0.6 m). Three to four sensor locations were selected in each canyon. Additional control sensor locations were selected in the unburned areas. Sensors were installed in half of these locations and will be installed in the remaining locations in summer 2025. Additionally, a standalone tipping bucket rain gauge will be installed in each canyon. A hand auger was used to drill a borehole in each sensor location and the sensors were placed horizontally as described in Akin et al. (2023). The sensors were connected to ZL6

data loggers (Meter Group, Pullman WA) and the data was recorded in each 15 min to 1 h increment. Bulk soil was collected from each location to calibrate the sensors in the laboratory.

Debris flow monitoring stations are planned to be installed at approximately 5 sites. These instruments will continuously record data over the duration of the study, capturing real-time information on seismic activity, precipitation patterns, and debris flow events. Similar installation configurations have been deployed by the USGS (Rengers et al. 2023, Fig. 2.61). A debris flow monitoring station consists of two geophones wired to a datalogger installed on a hillside near a channel. The datalogger is powered by a 12-volt battery located inside an enclosure. The enclosure, a solar panel, and a rain gauge are mounted to a ~2" diameter pole that is pounded into the ground. A pole-mounted solar panel charges the battery. Each geophone has a ~4" spike that is pushed into the ground. A time lapse camera is also connected to the datalogger and either mounted on the pole, a nearby tree or a t-post that is pounded into the ground. These are temporary installations that will be completely removed when the field monitoring portion of the study is completed. Please see photos of a similar installation deployed by the USGS (Rengers et al. 2023).
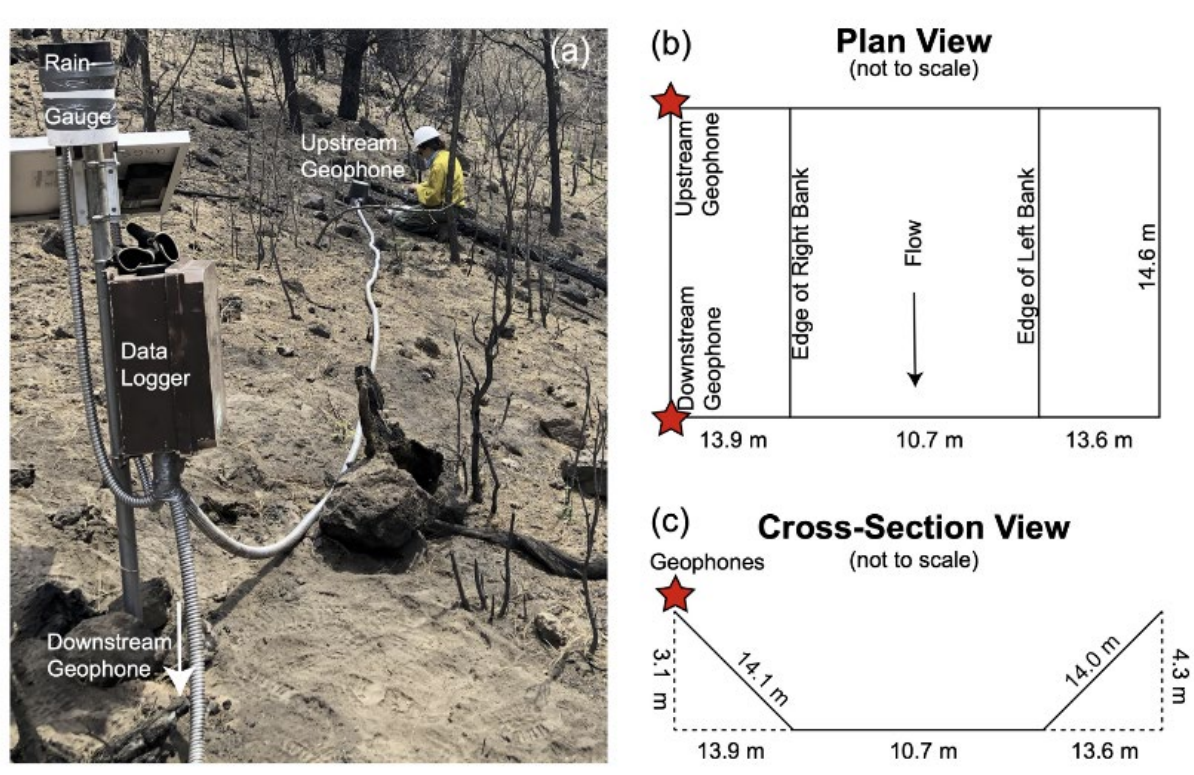

Fig. 2.61: Example of a debris flow monitoring station (Rengers et al. 2023).

3. Eaton Fire

3.1. Geology

The Eaton Fire burn area is located in the Altadena/Pasadena area within the western portion of the San Gabriel Mountains, also part of the Western Transverse Ranges. Surficial materials in the Eaton Fire burn area primarily consist of alluvium and weathered rock derived from the underlying crystalline bedrock. The bedrock is composed primarily of Mesozoic and Paleozoic age granitoids alongside some Precambrian igneous and metamorphic complexes (Jennings et al. 2010). The San Gabriel Mountains are bounded on the south by the Sierra Madre-Cucamonga fault zone, a major active fault in the region that produced the M6.6 San Fernando earthquake in 1971 (Treiman 2000).
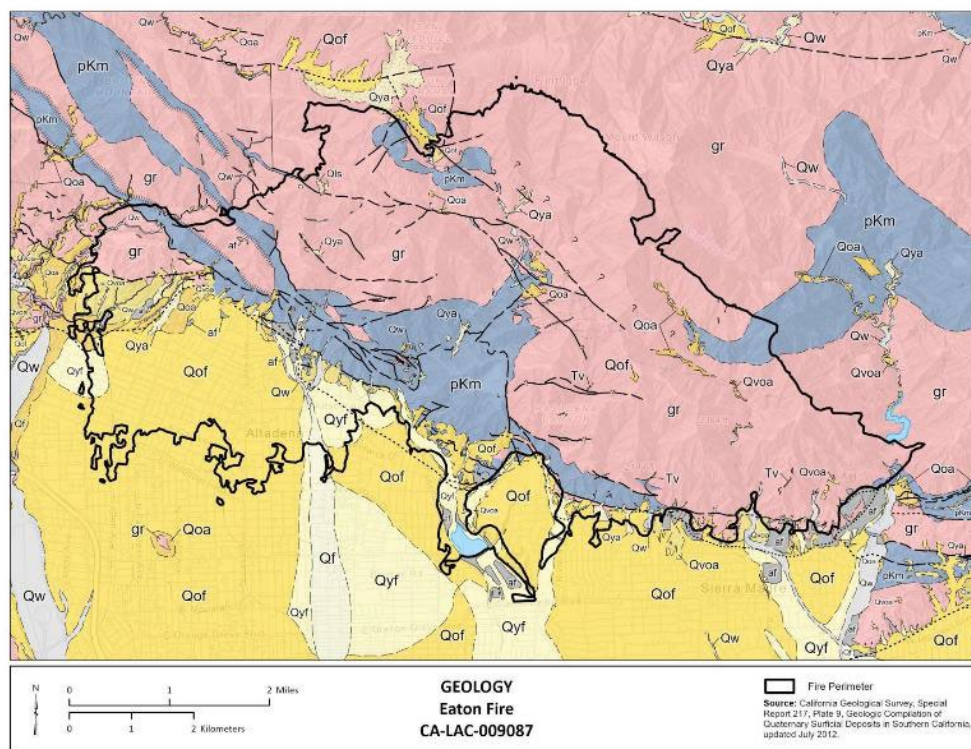
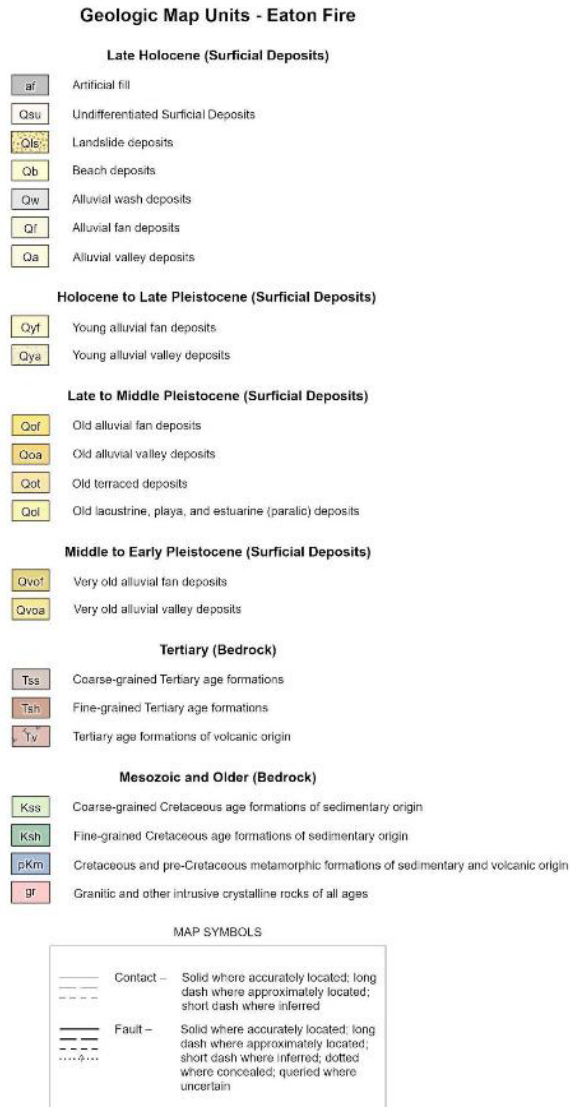**Fig. 3.1.** Geology map of the Eaton Fire burn area.

Geologic Map Units - Eaton Fire

Late Holocene (Surficial Deposits)

af	Artificial fill
Qsu	Undifferentiated Surficial Deposits
Qls	Landslide deposits
Qb	Beach deposits
Qw	Alluvial wash deposits
Qf	Alluvial fan deposits
Qa	Alluvial valley deposits

Holocene to Late Pleistocene (Surficial Deposits)

| Qyf | Young alluvial fan deposits |
| Qya | Young alluvial valley deposits |

Late to Middle Pleistocene (Surficial Deposits)

Qof	Old alluvial fan deposits
Qoa	Old alluvial valley deposits
Qot	Old terraced deposits
Qol	Old lacustrine, playa, and estuarine (paralic) deposits

Middle to Early Pleistocene (Surficial Deposits)

| Qvof | Very old alluvial fan deposits |
| Qvoa | Very old alluvial valley deposits |

Tertiary (Bedrock)

Tss	Coarse-grained Tertiary age formations
Tsh	Fine-grained Tertiary age formations
Tv	Tertiary age formations of volcanic origin

Mesozoic and Older (Bedrock)

Kss	Coarse-grained Cretaceous age formations of sedimentary origin
Ksh	Fine-grained Cretaceous age formations of sedimentary origin
pKm	Cretaceous and pre-Cretaceous metamorphic formations of sedimentary and volcanic origin
gr	Granitic and other intrusive crystalline rocks of all ages

MAP SYMBOLS

Contact – Solid where accurately located; long dash where approximately located; short dash where inferred

Fault – Solid where accurately located; long dash where approximately located; short dash where inferred; dotted where concealed; queried where uncertain

Fig. 3.1 (continued). Description of geologic map units for the Eaton burn area.

3.2. History of regional fires, landslides, and debris flows

Numerous historical fires have occurred within and in the vicinity of the Eaton Fire perimeter (Fig. 3.2). Although mapped fire perimeters in the area date back to at least 1911, most of the Eaton Fire burn perimeter has burned in the last half of the 20th Century, except for the far west portion in the Altadena foothills, which had not burned since the 1939 Las Flores #57 Fire. Three large fires (Monrovia Peak, Mountain Trail, and Pinecrest) burned the area in 1954, 1978, and 1979, respectively. The most recent large fire across most of the mountain front was the 1993 Kinneloa Fire, which burned the central portion of the Eaton Fire burn area from Altadena to the western edge of Sierra Madre. The 1999 Santa Anita II Fire burned the eastern edge above the Arcadia

foothills, and the 2008 Santa Anita Fire burned most of the foothills of Sierra Madre. The Eaton Fire burned approximately to the edge of the 2020 Bobcat Fire to the northeast and the 2009 Station Fire to the northwest.
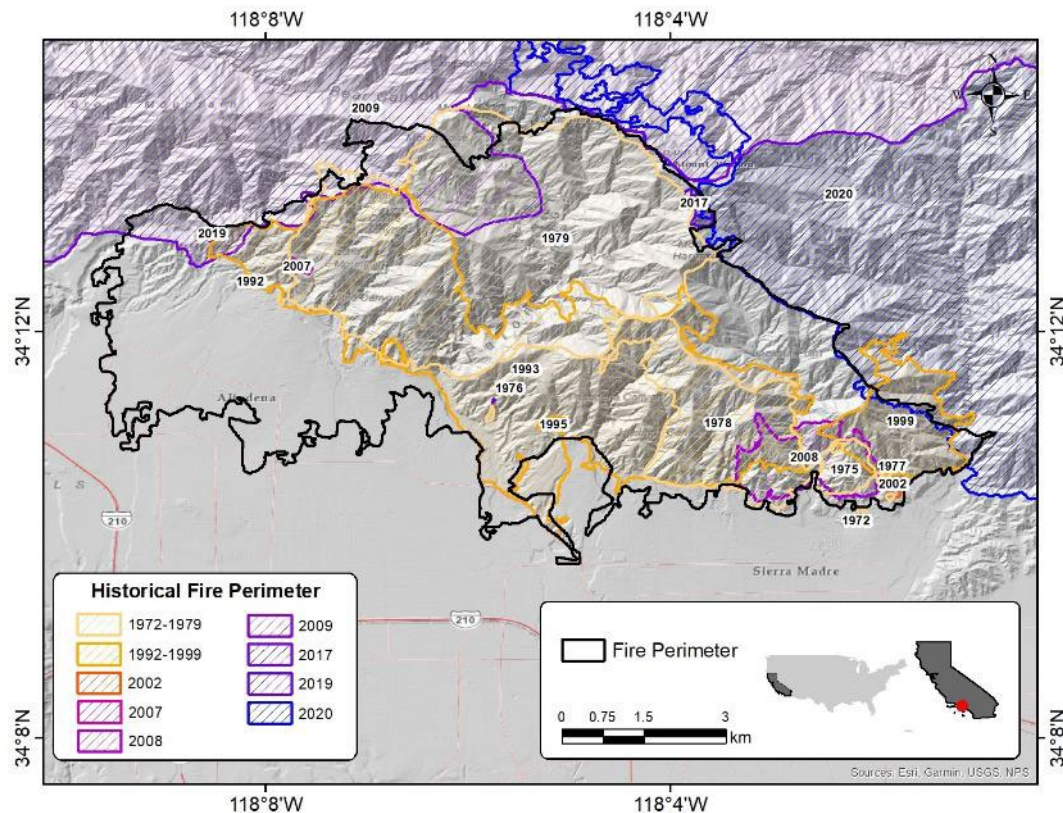

Fig. 3.2. Eaton Fire perimeter (black) and historical fire perimeters in the area.

The San Gabriel Mountains and the underlying igneous and metamorphic rocks generally support steep slopes in the Eaton fire burn area that are prone to rockfall and shallow and deep-seated landslide processes. Landslide mapping within the burn area (Fig. 3.3) show a variety of landslides ranging from dormant-old, moderate- to deep-seated rotational/translational failures to active shallow-seated debris slide failures. Postfire effects can increase landslide activity, generally 3 to 5 years following fire (Rice and Foggin 1971, Rengers et al. 2020), causing existing failures to reactivate or new failures to develop, particularly in steep colluvial-filled hallows. This increase in landslide activity can be attributed to a reduction in root strength (Vergani et al. 2017) and altered surface and shallow subsurface hydrology.
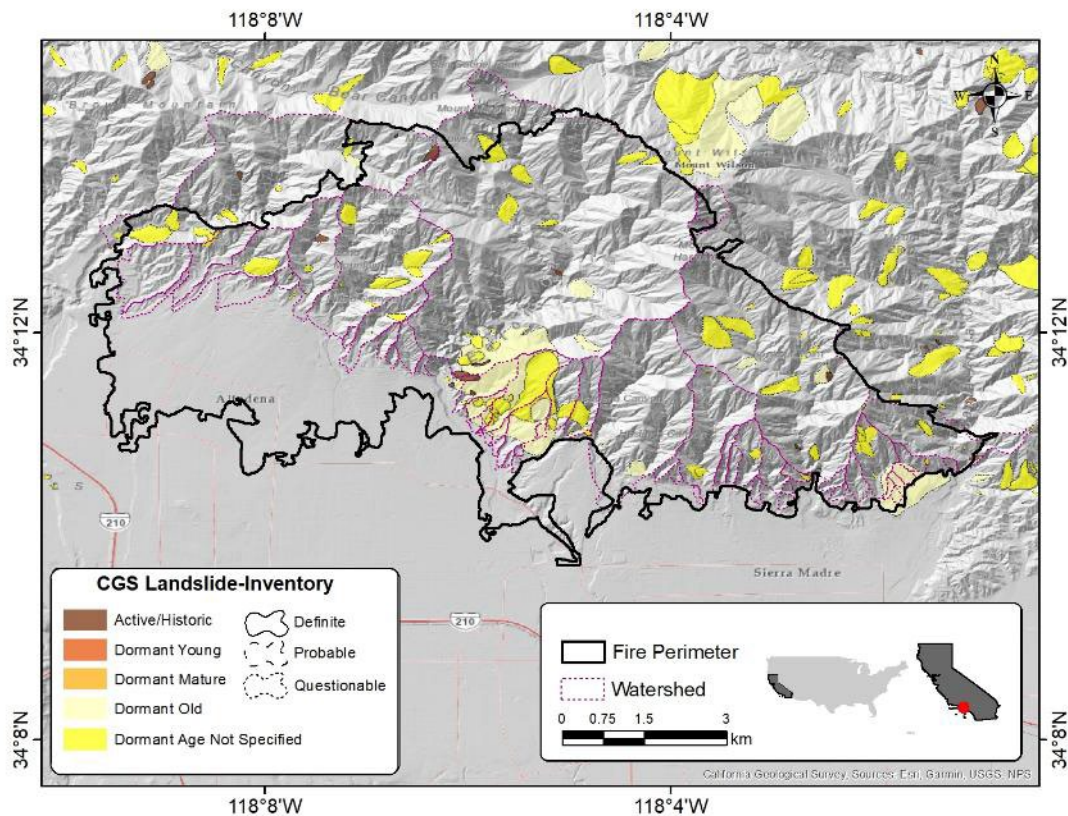
Fig. 3.3. Historic landslides in the Eaton Fire burn area.

There are several documented post-fire debris flows within or immediately down gradient of the Eaton Fire perimeter in recent history (since 1980). The closest confirmed, recent post-fire debris flows were documented in 1980 following the 1979 Pinecrest Fire with reports of debris flows and floods occurring within Pasadena Glen and Rubio Canyon after 279 mm of rain fell within a 24-hour period. Debris entering the Rubio Canyon Debris Basin caused it to overtop and lead to homes being flooded along Gooseberry Lane, Sunny Oaks Circle, and Altadena Drive (Manning, 1993).

Additional postfire flood and debris flow activity was reported following the 1993 Kinneloa Fire, which triggered a debris flow in Bailey Canyon and led to approximately 2000 cubic yards of debris to infill Kinneloa debris retention basin (Cannon et al. 2010). An additional debris flow impacted Pasadena Glen after the same fire (Sullivan 1994). The most recent reported postfire debris flows occurred following the 2008 Santa Anita Fire, which produced low-volume debris flows in at least one watershed, as reported by the National Weather Service (Cannon et al 2008).

Other recent fires with documented post-fire debris flows further from the Eaton Fire, but within the San Gabriel Mountains, include the 2009 Station Fire (> 109 post-fire debris flows) and the 2016 Fish Fire (7 post-fire debris flows, Staley et al. 2016). The environmental settings of these

fires are very similar to that of the Eaton Fire, therefore similar responses are likely for areas impacted by the Eaton Fire. The USGS debris flow model estimates more than 80% likelihood of debris flows in all the watersheds in the Eaton fire perimeter (Fig. 3.4).
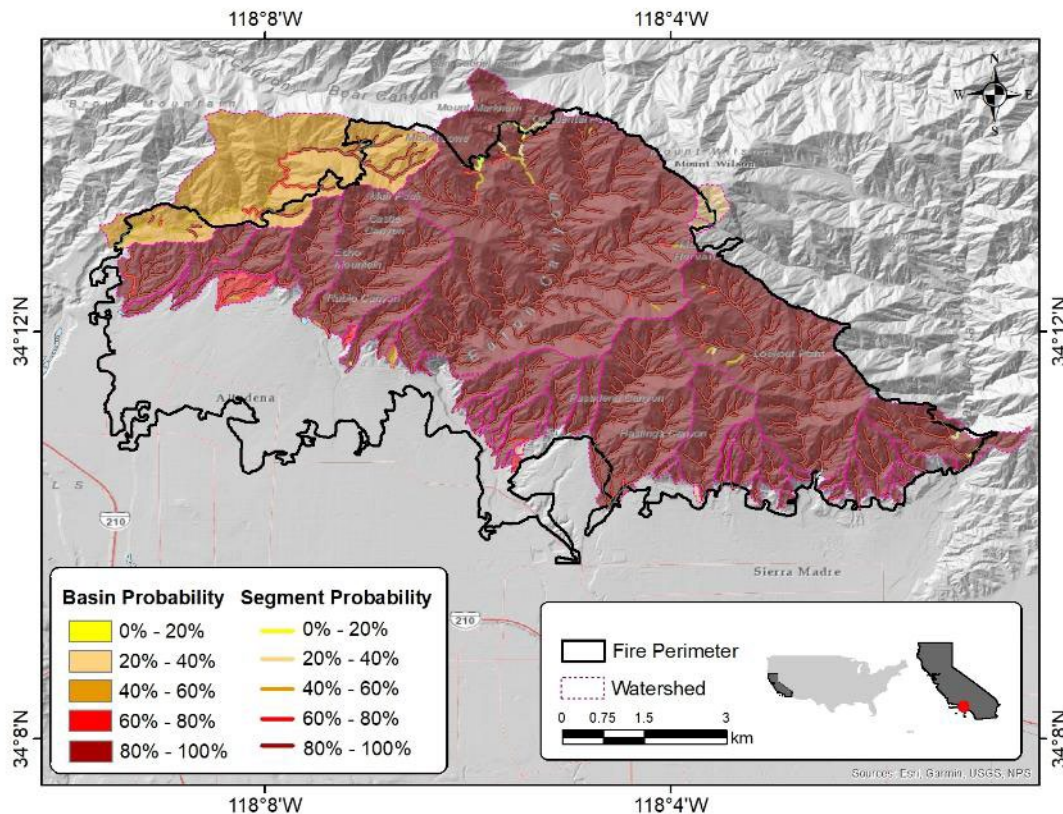
Fig. 3.4. Debris flow likelihood at the Palisades Fire (40 mm/h storm) according to USGS debris flow model (Staley et al. 2017).

3.3. Imaging

High resolution images of debris basins were obtained using an UAV system as described in Section 2.3 with minor differences. For RTK corrections the Emlid Reach RS3 was used, which is a multi-band GNSS receiver that provided reliable base station support to maintain centimeter-level positioning accuracy. To sustain extended field operations, the team relied on the DJI BS65 Intelligent Battery Station paired with five sets of DJI TB65 batteries. A portable power generator was also deployed to recharge batteries in the field, allowing for continuous data acquisition by alternating battery usage efficiently.

All LiDAR data were processed using DJI Terra software, which facilitated point cloud generation, LiDAR frame alignment, and bare-ground classification. Surveys were conducted at flight altitudes between 100 and 120 meters above ground level, employing the UAV's terrain-

following feature to maintain a consistent ground sampling resolution. This approach achieved a spatial resolution of approximately 3.5 cm per pixel and yielded point densities ranging from 500 to 700 points per square meter. To ensure sufficient coverage and minimize data gaps, we established an 80% front overlap and a 20% lateral overlap between data frames. Additionally, RGB imaging was enabled during all flights, providing color information for point cloud visualization. The UAV operated at a maximum speed of 15 meters per second, with an average survey speed maintained at approximately 6 meters per second to optimize data quality.

3.4 Debris retention systems

To protect developed areas against flood and debris flows, the Los Angeles County Public Works along with state and federal partners, have constructed an elaborate network of flood and sediment control measures that include debris basins, elevated inlet structures, and desilting inlet structures. Many of these flood and sediment control measures were initiated following large flood events that impacted southern California in 1938 and 1969, and the construction and maintenance of structures has continued (Fig. 3.5).
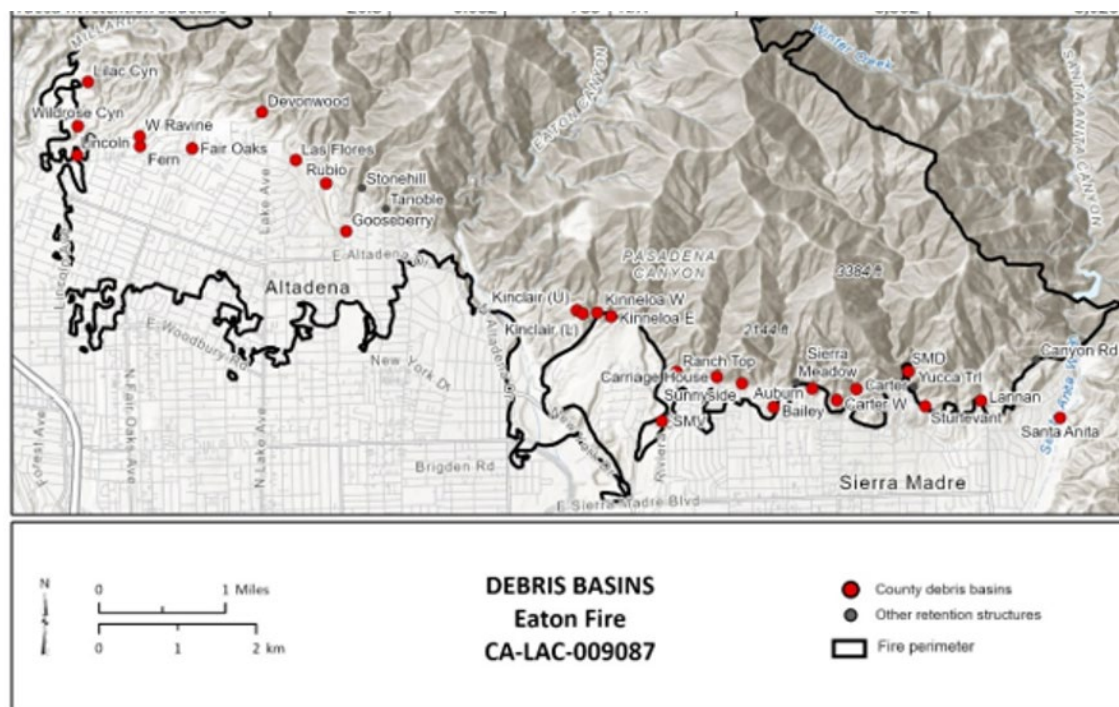
Fig. 3.5. Debris basins in the Eaton fire burn area.

Common types of flood and debris flow control structures observed by the team include debris basins, desilting inlets, crib dams and rail and timber structures (Fig. 3.6). Many of these structures are intended to allow sediment and debris to be trapped while allowing water to flow into downstream flood control systems. Only debris basins are designed to accommodate the

Design Debris Event (DDE), which is defined as the quantity of sediment produced by a saturated watershed significantly recovered from a burn (after four years) as a result of a 50-year, 24-hour rainfall amount (Wolfe 2006).

Debris Basin - typically composed of a drainage standpipe and an emergency spillway with debris barrier. Typically designed to accommodate the Design Debris Event. Photos is of the Kinneloa West debris basin. (34.1835°; -118.0858°) 	Crib Dam Structure - intended to trap sediment, reduce channel gradient, and promote deposition upstream. Note intended to contain the Design Debris Event. (34.19831°; -118.11786°)
Debris Barrier - typically used to trap large material composed of boulders and woody debris while allowing fine-grained material to pass. (34.17586°; -118.07206°) 	Rail and Timber Structure - intended to trap sediment and debris while allowing water to pass. Not designed to contain the Design Debris Event. (34.19588°; -118.11459°)

Fig. 3.6. Examples of flood and debris flow control structure.

3.5. Post-fire precipitation events

The area burned by the Eaton Fire has a Mediterranean climate and the hydrology of the area is governed by rainfall. According to rainfall data from representative gauges in the burn area, or vicinity, the Eaton Fire was impacted by three storms starting with the first rainfall after the fire on January 25-26, 2025 (Fig. 3.7) (Precipitation data were obtained from Synoptic Data using the Weather API (Synoptic 2025) and from the Weather Underground Wundermap application (Wunderground 2025). As shown in Fig. 3.7, those data indicate a wide range of rain accumulation over the burn area from about 7 mm to above 27 mm. Subsequent rain events on February 13, 2025, and March 13, 2025, were more spatially uniform with rain accumulations of above 90 mm and 37 mm on average, respectively.
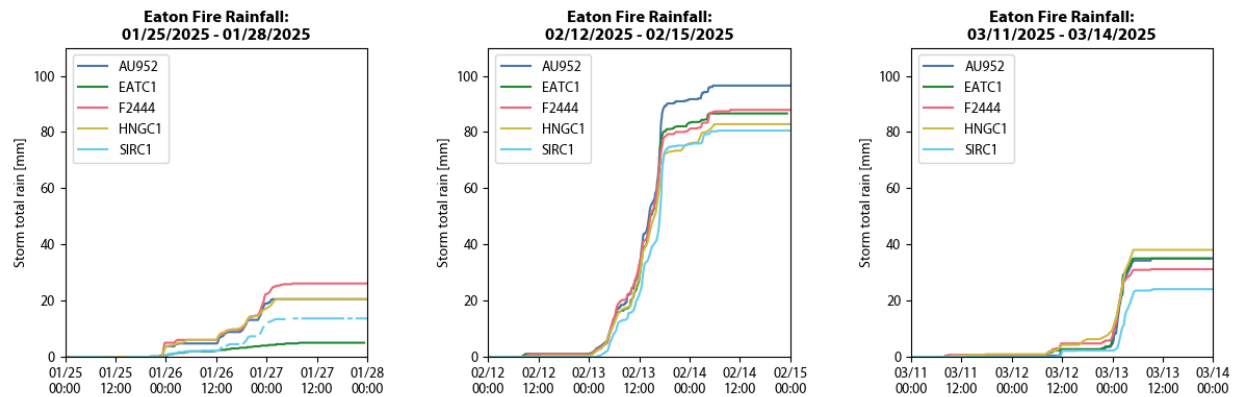
Fig. 3.7. Rainfall accumulation data for three storms impacting the Eaton Fire. See Fig 1.4 for gauge location.

The 15-min and 60-min peak rainfall intensity data during the January 26th, February 13th, and March 13th storms were gathered from all rain gauges in the vicinity of the fire perimeter (Fig. 3.8). The 15-min peak rainfall intensity reached 49 mm/h during the February 13th storm. Peak 15-min rainfall intensities across the burn area had an average annual recurrence interval of about 1-2 years, according to National Oceanic and Atmospheric Administration (NOAA) Atlas14 (Perica et al. 2014).
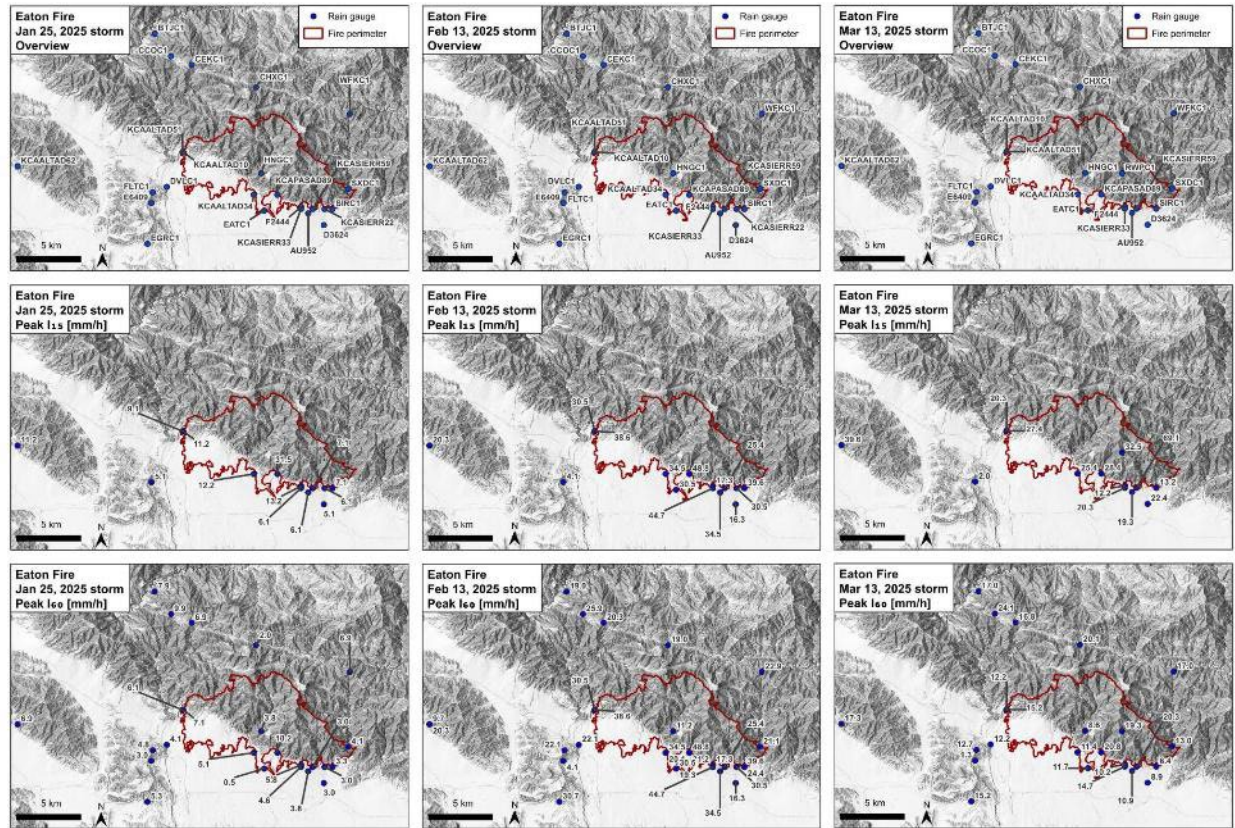
Fig. 3.8. Rainfall distribution across the Eaton Fire for three storm events

3.6. Erosion, Debris Flows, and Landslides

3.6.1. Erosion

Dry raveling immediately following the Eaton fire was observed throughout the burn area. Ravel cones were observed infilling low order channels with up to several meters of mostly coarse, cohesionless sand material (Fig. 3.9). Due to the mostly granitic bedrock underlying the Eaton Fire and the corresponding supply of friable sand-rich material, the presence of dry ravel, both spatially and volumetrically, appeared greater in the Eaton Fire compared to the Palisades Fire.

Using two Digital Elevation Models (DEMs) surveyed before (2016) and after the fire (January 22, 2025) with a spatial resolution of 1 m per pixel, Brigham et al. (2025) calculated a differential Digital Elevation Model (dDEM, Fig. 3.10). The resulting dDEM highlights areas with decreased elevation caused by erosion (red), and the ravel sediment deposits (blue).

Fig. 3.9. Typical post-fire dry-ravel deposit within first order drainage. Date 1-17-2025. (34.19523°, -118.11264°).
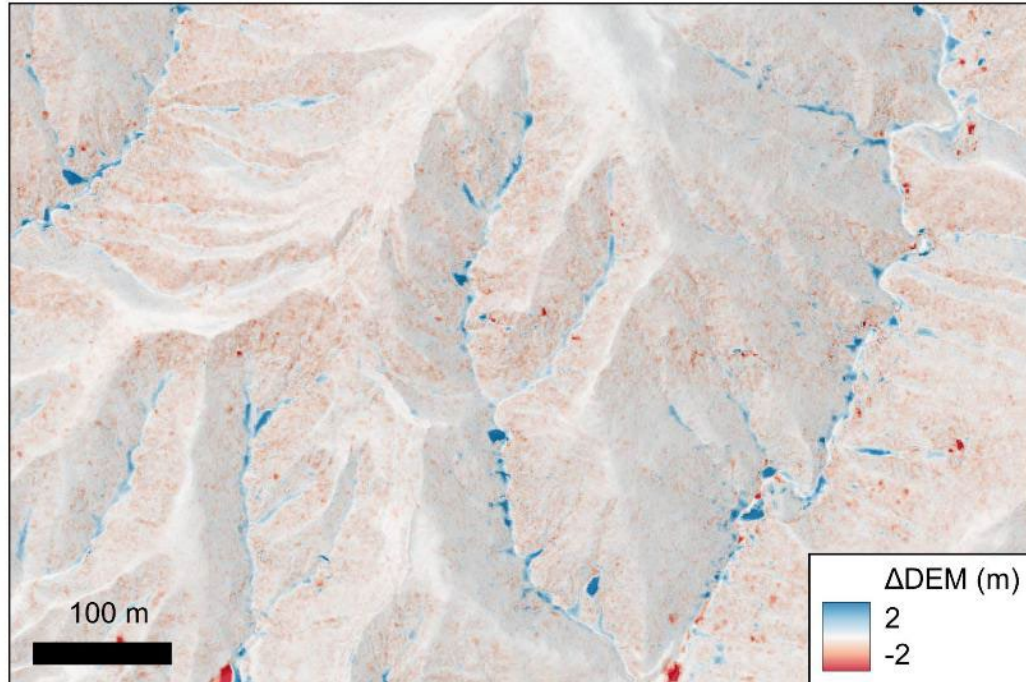

Fig. 3.10. Digital elevation map differences (dDEM) in and immediately west of Bailey Canyon from airborne lidar DEM difference from 2016 to January 22, 2025, before and after the Eaton Fire (data from Brigham et al., 2025). Note that 0-2 m of postfire dry ravel was deposited in the channels.

Minor rilling was observed following the January storm with more extensive rilling and scour of ravel cones and channel deposits observed following the February storm (Fig. 3.11).

Fig. 3.11. Typical coalescing ravel cones entering channel within the Eaton Fire (34.1768°, 118.0611°).

3.6.2. Debris Flows/Debris Floods

Following the same characteristics differentiating flood flows, debris floods and debris flows outlined in Section 2.7.2, postfire runoff response from the February and March storms was documented through personal accounts, reports by colleagues, and media reports. The type of runoff response, ranging from flood flow to debris flow, and their spatial distribution is shown for the Eaton fire in Fig. 3.12. In addition, depth of deposits and maximum grain size were recorded in areas where overbank flows occurred. We did not perform a post-storm response following the January 25, 2025 storm and we are unaware of such a response from other teams.
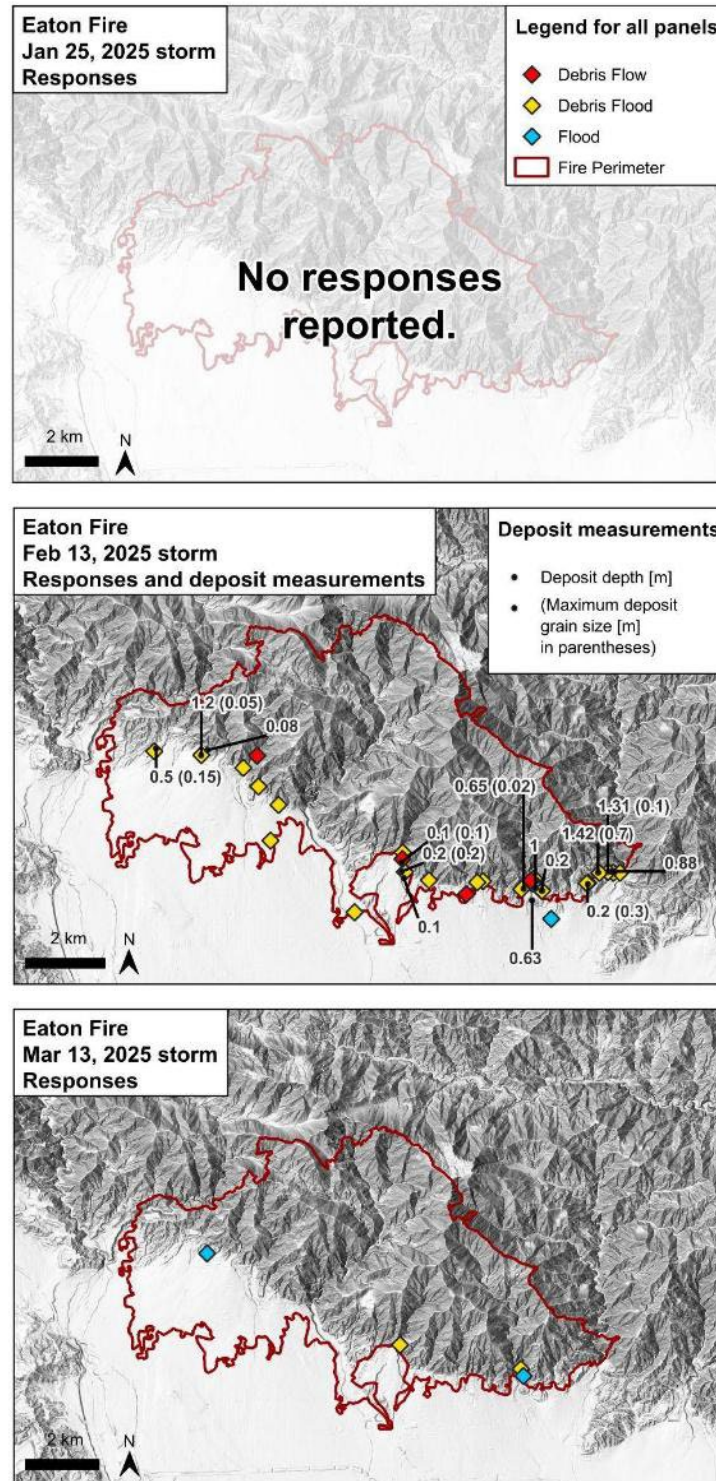
Fig. 3.12. Observed flow responses at the Eaton Fire for the January 25, February 13, and March 13 storms. Points are colored by flow type and located at the basin outlet where the observation was made. The February 13 response map also includes several measurements of deposit depth and maximum grain size observed in the deposit.

During the February 13, 2025, storm, many of the debris basins were filled with debris to their capacity, while some overspilled causing property and infrastructure damage. Members of the GEER team from Caltech monitored some debris basin capacities after the fire, after subsequent rain events, and after LA County clean-out efforts. Measurements were made through repeat UAV based lidar surveys and were made available to emergency management [LA County and CGS] within days of data collection to aid in hazard mitigation (Fig. 3.13). The results are intended to support emergency management agencies by (i) prioritizing debris basin cleanouts, (ii) calibrating and validating debris flow models for the burned catchments, and (iii) forecasting potential debris flow risks for upcoming storm events. These analyses can be used to inform where basins are lacking in capacity to protect downstream communities and allow models to be updated as basins are filled by consecutive storms.
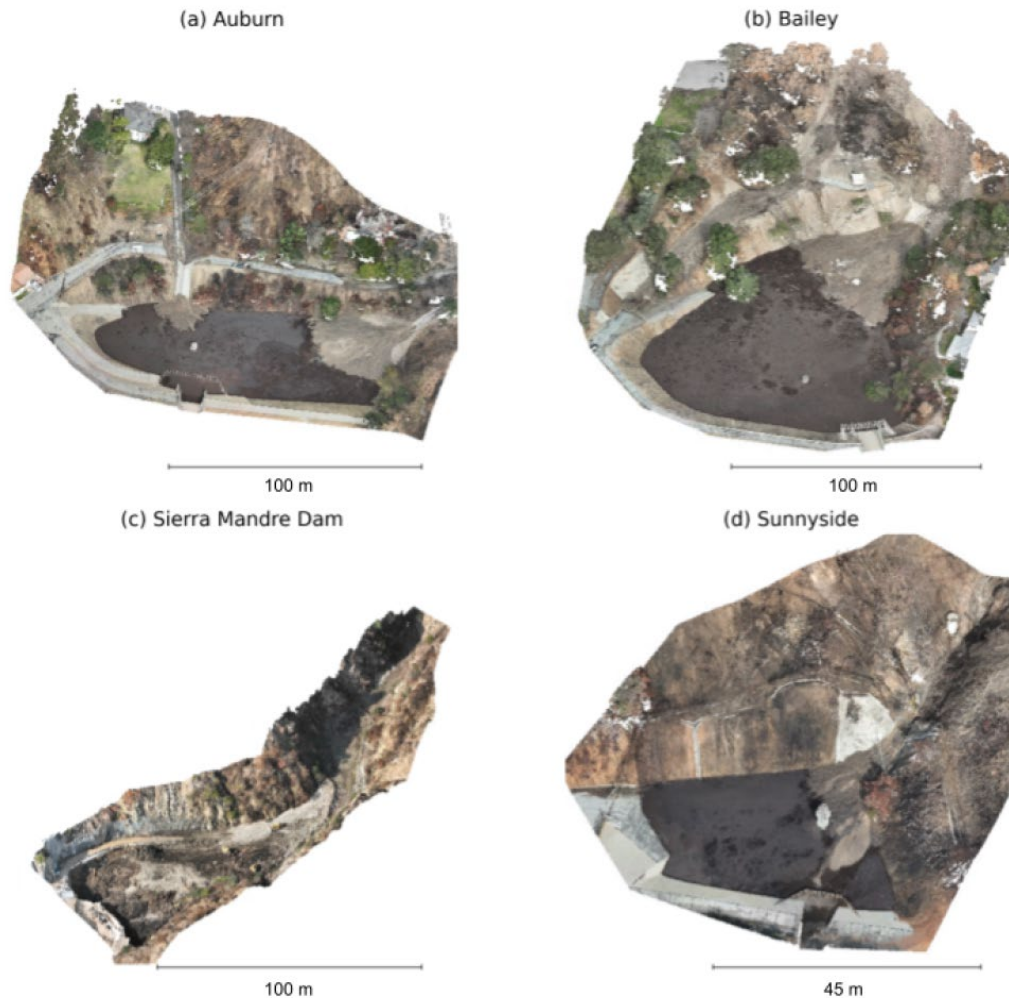

Fig. 3.13. Example point clouds from UAV lidar surveys of debris basins: Auburn, Bailey, Sierra Madre Dam and Sunnyside.

For some basins, repeat surveys were conducted following a single storm to assess if significant dewatering had occurred (i.e., to better measure debris volumes vs. water volumes). We found that the Feb 13-15, 2025 storm event delivered approximately 480,000 cubic yards of debris to the 14 surveyed basins, filling the basins to amounts ranging from 12 to 59% of their design capacities (Fig. 3.14). Preliminary results description and data from this study can be found in Chen et al. (2025) [see "data_description.pdf" therein for a summary report"].
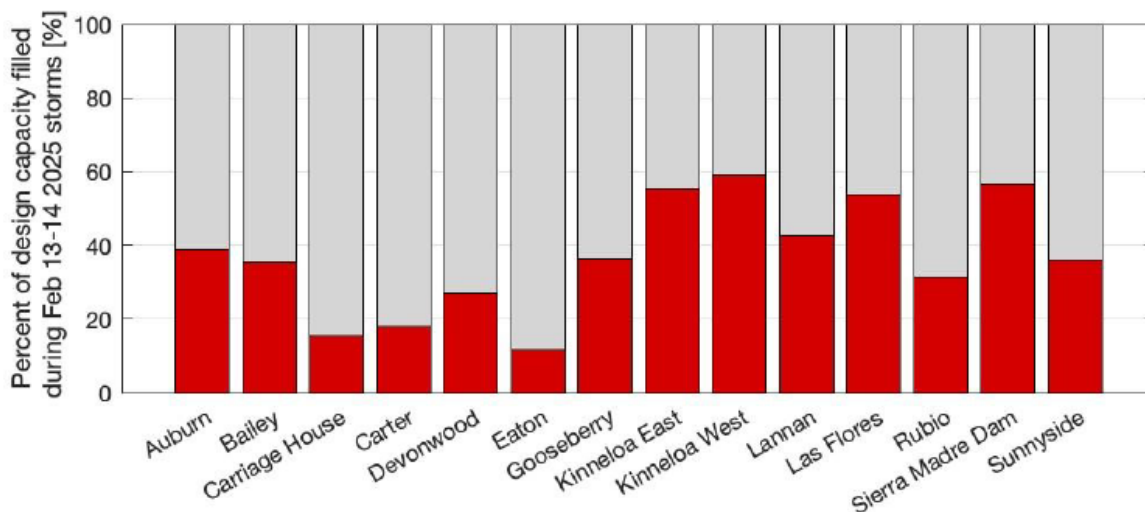

Fig. 3.14. Measured debris volumes delivered to each basin during the Feb. 13-14 storm event, plotted as a percent of each basin's total design capacity.

3.7. Damage to Infrastructure Systems

3.7.1. Water

Damage to Kinneloa Irrigation District water supply lines and infrastructure was observed including, damaged well heads, fencing and access roads, was observed in several locations, such as in Pasadena Glen and Rubio Canyon (Fig. 3.15-3.17).

Fig. 3.15. A bridge across Rubio Canyon that accesses a Kinneloa Irrigation District well head. (1/18/25, 34.18385°, 118.12288°).

Fig. 3.16. Damage to the bridge and associated fencing (2/19/25, 34.18385°, 118.12288°).

Fig. 3.17. Image showing damaged Kinneloa Irrigation District waterline (opposite bank) within Pasadena Canyon. Several waterlines of different ages exist along this reach. Observed damage occurred during the February 13th, 2025, storm. Photo taken on 2-20-2025. (34.18294°, 118.07856°).

3.7.2. Retention and Drainage Structures

Similar to the Palisades Fire, several forms of retention or drainage structures were damaged by the Eaton Fire, which may reduce their effectiveness. Burnt soldier pile retaining walls were observed across the fire at the foot of natural slopes (Fig. 3.18a), below roadways (Fig. 3.18b), and along a channel adjacent to a residential property (Fig. 3.18c).

Fig. 3.18. Evidence of burnt soldier pile retaining walls at the Eaton Fire a) at the foot of a natural slope, b) below a roadway, and c) adjacent to a residential property. (Top: 34.176998°, -118.019583°; lower left: 34.176234°, -118.030142°; lower right: 34.194497°, -118.112748°)

Along Santa Anita Canyon Road, a plastic culvert running under the road and into a steep channel below the road had fully melted, leaving an unlined tunnel of exposed soil below the road (Fig. 3.19a). At this same location, heat from the burning culvert and surrounding fire was directed through the culvert and out of the upstream end, causing substantial spalling of the concrete

debris retention structure. The quantity of spalled material was enough to almost completely block the drain grate (Fig. 3.19b), potentially reducing the flow capacity of the culvert.

(a)

(b)

Fig. 3.19. (a) Melted culvert and (b) subsequent spalling of concrete debris retention structure along Santa Anita Canyon Rd. (34.177282°, -118.029274°).

3.8. Field Instrumentation and Long-Term Monitoring

One telemetered rain gauge and three debris flow monitoring stations were installed for the Eaton Fire (locations provided in Fig. 1.4). These instruments will continuously record data over the duration of the study, capturing real-time information on ground movement, precipitation patterns, and flow events, similar to installations deployed by the USGS (Rengers et al. 2023, Fig. 2.61). The main monitoring site at Pasadena Glen (Fig. 3.20), operated by CGS consists of geophones, radar-based non-contact stream stage and velocity sensors, in-channel pressure transducers, camera, and tipping-bucket rain gauges at the outlet and headwaters of the basin. Another monitoring station at Stonehill operated by CGS and USGS consists of geophones, a non-contact stage sensor, video camera, and a tipping-bucket rain gauge. A video camera and tipping-bucket rain gauge were also installed at Rubio Canyon by USGS.

Fig. 3.20. Overview of equipment installed at the Pasadena Glen monitoring site.

Because the equipment was installed the week of February 18, CGS estimated flow data for the February 13 storm using video analysis methods. At Pasadena Glen, several video cameras were installed by a resident and flow velocity and stage were estimated from the video, and a hydrograph (Fig. 3.21) was constructed based on the surveyed channel cross-section.
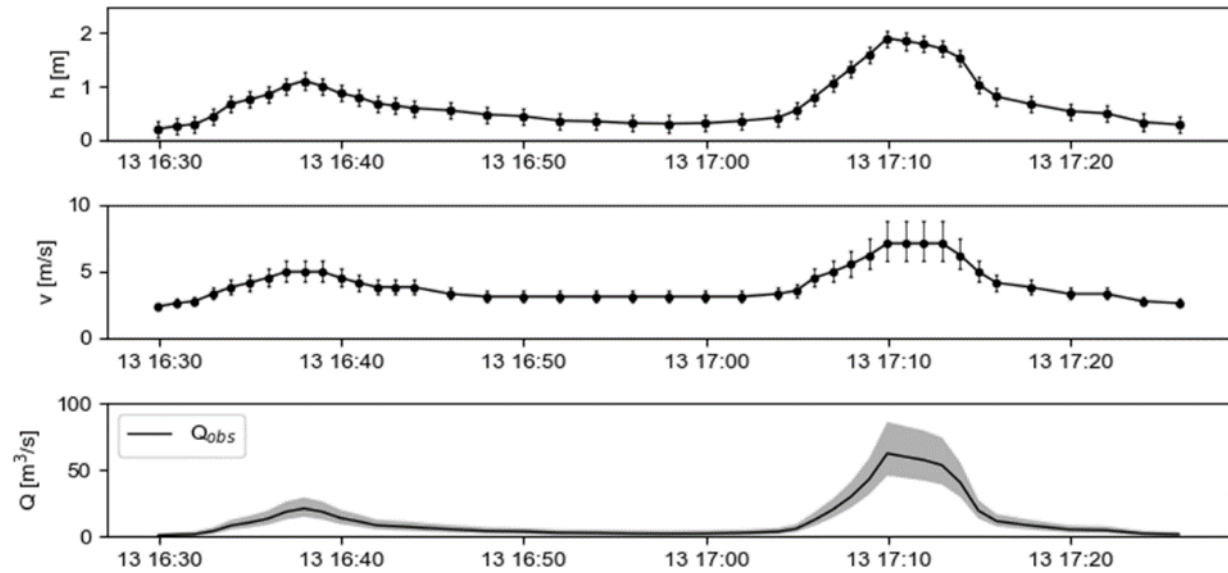
Fig. 3.21. Flow data (stream stage h, surface velocity v, and discharge Q) at Pasadena Glen during the peak of the February 13 flow event, estimated from video of channel.

At the Bailey debris basin, a video camera installed by AlertCalifornia (https://alertcalifornia.org/) captured the rapid filling of the basin. The Bailey debris basin is composed of an earthen dam with a concrete-lined spillway and a vertical drainage standpipe. Assuming the standpipe was plugged during the runoff event, a hydrograph (Fig. 3.22) was constructed by estimating the elevation of the water surface through time, using this water surface elevation and the basin's hypsometry to estimate the stored volume in the basin, and computing the derivative of stored volume with respect to time to estimate discharge. The assumption that the drainage rate through the standpipe was negligible appeared reasonable, based on subsequent field observations indicating the presence of standing water remaining in the basin after flows entering the basin stopped and evidence in the video.

For the March 13 storm, data was directly measured at Pasadena Glen (Fig. 3.23) and Stonehill (Fig. 3.25) by the installed non-contact monitoring equipment. At Pasadena Glen, the equipment recorded rainfall, presented as cumulative rainfall and rainfall intensity over a 15-minute duration, seismic shaking (mV), stream stage, and stream surface water velocity (Fig. 3.23). To estimate discharge at different stream stages, the wetted cross-sectional area at each stage was multiplied by the average stream velocity at the same stage. The average stream velocity was approximated by multiplying the average surface water velocity recorded at the corresponding stage by 0.85 (Fig. 3.24).
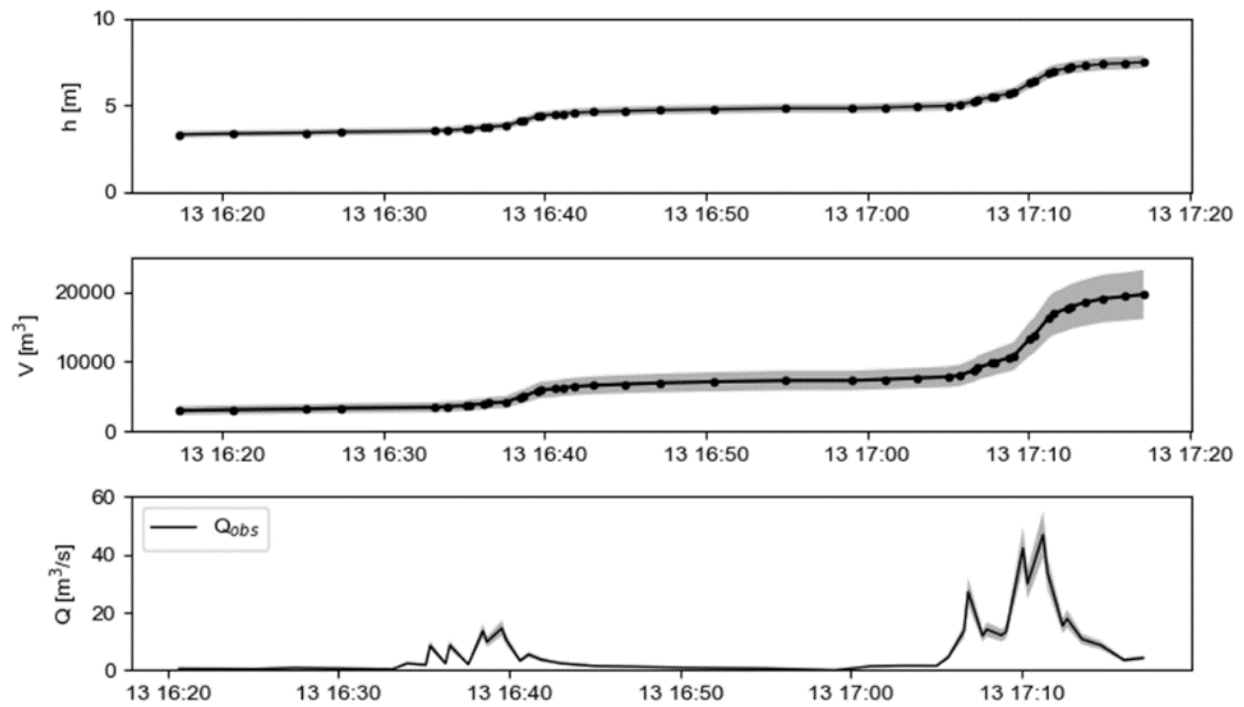
Fig. 3.22. Flow data (water surface elevation h, stored volume V, and discharge Q) at Bailey Canyon during the peak of the February 13 flow event, estimated from video of debris basin.
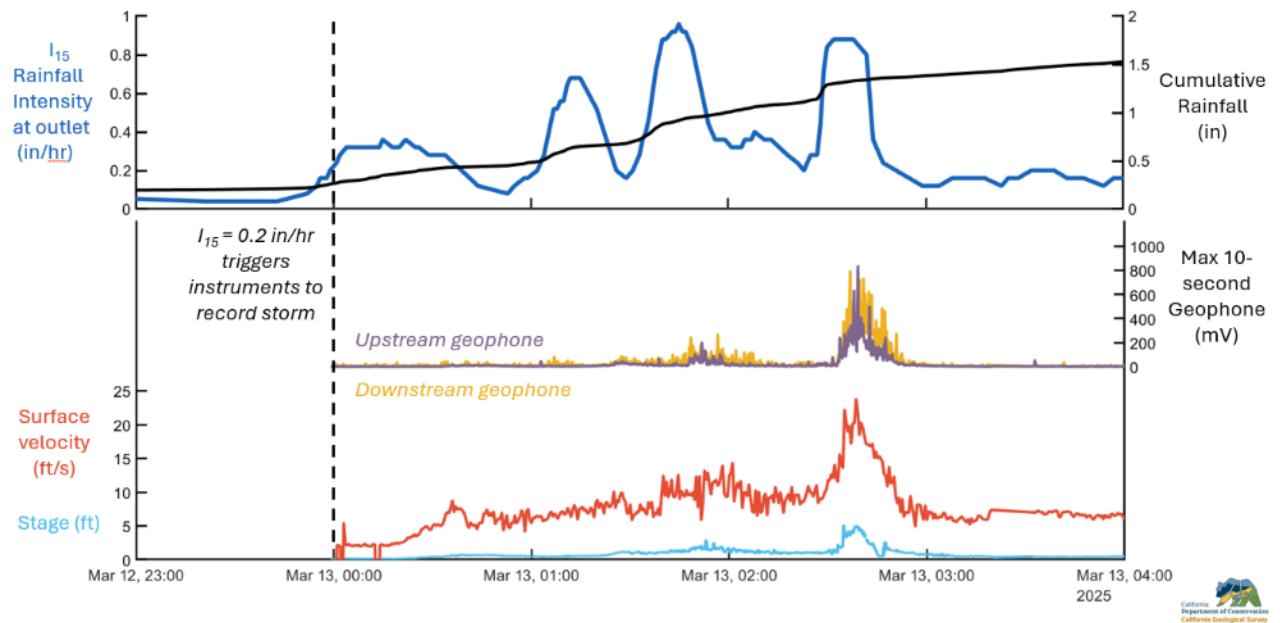

Fig. 3.23. Raw rainfall, seismic shaking, and stream stage and velocity data at Pasadena Glen during the March 13 flow event, as measured by the equipment.
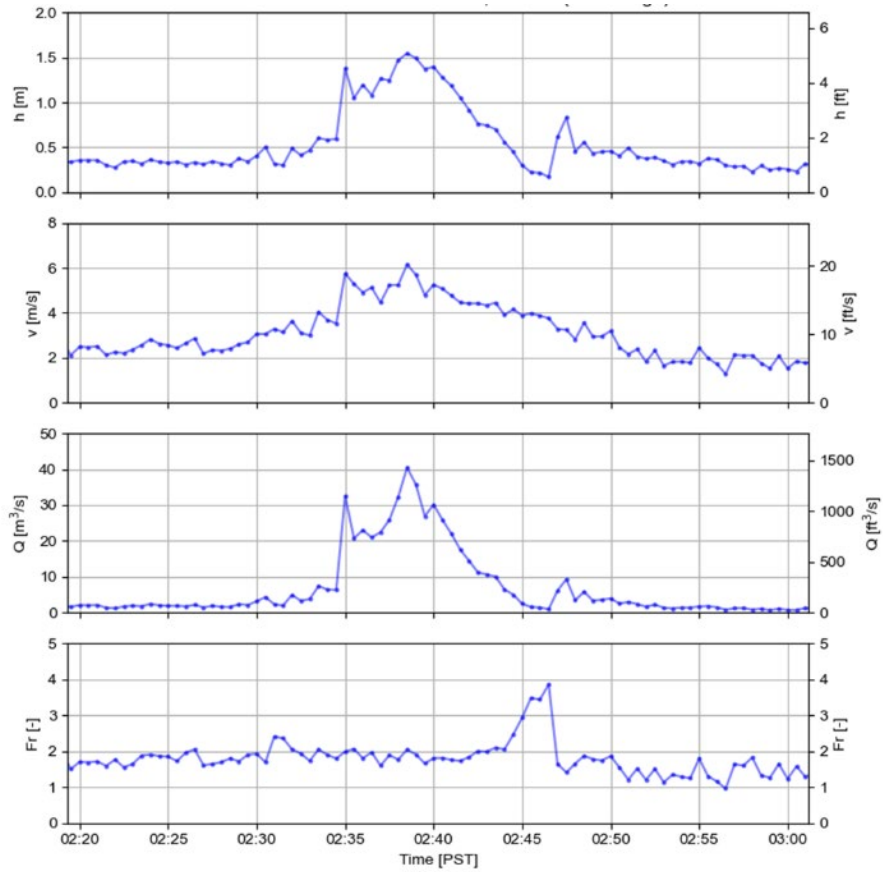
82

Fig. 3.24. Flow data (stream stage h, surface velocity v, discharge Q, and Froude number Fr) at Pasadena Glen during the peak of the March 13 flow event, as derived based on the channel wetted cross-sectional area and average flow velocity.

At Stonehill, the equipment recorded rainfall, seismic shaking (mV), and stream stage (Fig. 3.25). Stage data showed a rapid rise in flow over a short duration (Fig. 3.25), indicating the presence of a dilated flow front passing the monitoring station. This type of flow response is common in small to moderate-sized basins burned at moderate and high soil burn severity (Kean et al. 2011)
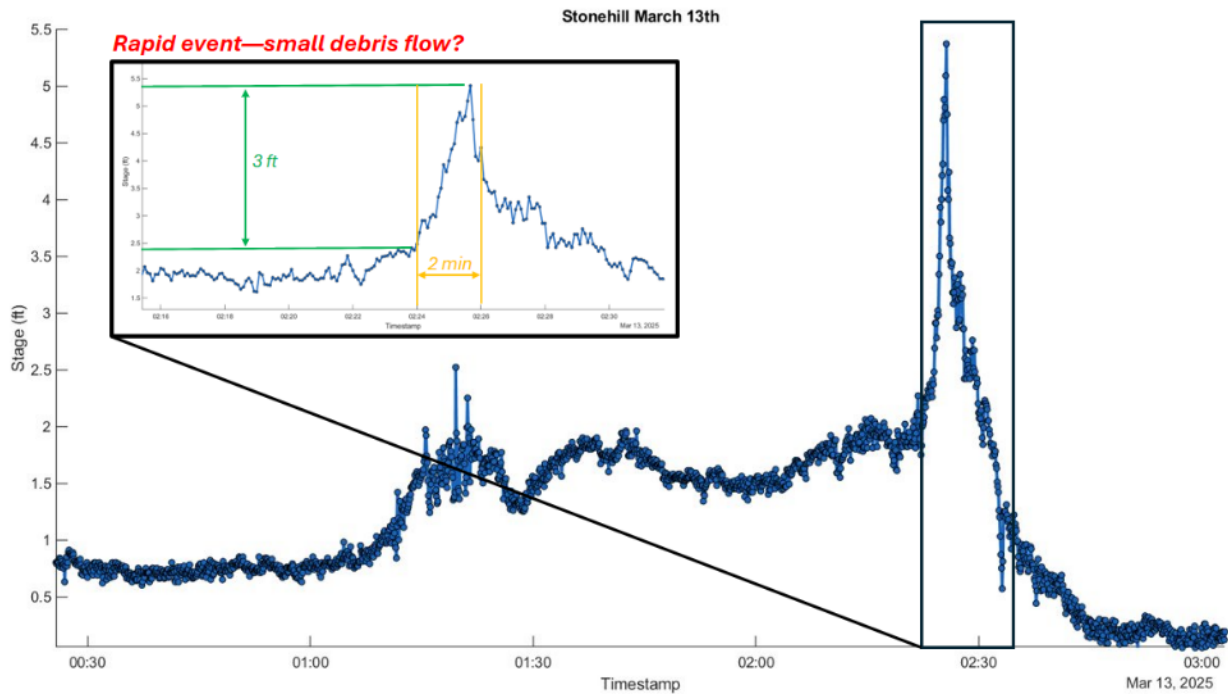
Fig. 3.25. Stream stage data at Stonehill during the March 13 flow event, as measured by the equipment.

3.9 USACE Hydrologic and Hydraulic Models

The USACE leveraged HEC-HMS and HEC-RAS modeling to evaluate post-wildfire flood risks within and downslope of areas impacted by the Eaton fire (USACE 2025). The USACE applied HEC-HMS to develop comprehensive watershed level rainfall-runoff models to compute the postfire flows for the 1/2, 1/5, 1/10, 1/25, 1/50, 1/100, 1/200, and 1/500 Annual Exceedance Probabilities (AEP) flood events for several principal channels in the burn area. The USACE then performed 2D hydraulic modeling using HEC-RAS (version 6.6) to perform hydraulic analysis that considered non-Newtonian flow effects to develop inundation maps and estimated sediment yields for the previously mentioned AEP flood events. Although the final report and accompanying maps and data are currently in review and have not been released, preliminary results suggest the information provided may support informed decision-making regarding emergency management planning and mitigation efforts.

4.0 Summary, Conclusions, and Future Work

This report presented the team's findings of the effects of Palisades and Eaton Fires on infrastructure, natural and man-made slopes, and vegetation. The reconnaissance teams conducted extensive aerial and ground-based campaigns. Aerial campaigns included drone- or plane-mounted LiDAR surveys and high-resolution imagery. Ground-based reconnaissance included scouting, sampling, and instrumentation. Damage to retaining structures, houses, storm drains, transmission lines, and roadways were documented in the residential areas.

The reconnaissance teams visited affected areas multiple times and monitored the slope instabilities after three storm events in January, February, and March 2025. Hillslopes showed signs of localized hydrophobicity and discontinuous ash layers that progressively covered a smaller surface after each storm event. Macropores that formed because of burned surface roots were common on the burned slopes. Dry ravel, widespread rilling, debris floods/flows, and landslides were documented at the sites. The January 25th storm resulted in multiple debris floods and a debris flow in the Palisades Fire burn area. The February 23rd storm resulted in the maximum sediment yield in both Palisades and Eaton Fire burn sites. Rills progressed into gullies, and more debris floods/flows occurred in the Palisades Fire burn area. Some debris basins at Eaton Fire burn area were filled to their capacity after the storm and some over spilled.

The teams identified unstable areas for long-term monitoring and will continue collecting data through remote sensing, in-situ testing, and instrumentation. The collected data will be analyzed to quantify surface movements and related changes in slope hydrology. As the slopes recover, the changes in hydrologic response of burned slopes and shallow slope instabilities will be documented.

Photos, track logs, and shapefiles representing drone flight coverage areas have been published (Akin et al. 2025) via the DesignSafe cyberinfrastructure (Rathje et al. 2017). Furthermore, a map presenting the data can be found at the following URL: URL: https://doi.org/10.17603/ds2-6g0m-xn64. The dataset will likely be amended in the future to include LiDAR point clouds, shapefiles representing aerial LiDAR flight paths, and observations of any future land movements.

The data collected from these events has the potential to support useful follow-up research, such as the development of models to predict post-wildfire hydrology and corresponding sediment movement through erosion, landslides, and debris flows, development of models for debris yield from drainages from storms following fire, and development of models for interactions of lifeline infrastructure systems during and after the fires and debris flows.

References

3D Elevation Program (2025). Post-wildfire lidar data for Los Angeles, CA: https://www.usgs.gov/3d-elevation-program/science/2025-post-wildfire-lidar-data-los-angeles-ca.

Akin, I.D., and Akinleye, T.O. (2021). Water vapor sorption behavior of wildfire-burnt soil, *J. Geotech. Geoenviron. Eng.*, doi: 10.1061/(ASCE)GT.1943-5606.0002648.

Akin, I.D., Akinleye, T., and Robichaud, P.R. (2023). Changes in soil properties over time after a wildfire and implications to slope stability, *J. Geotech. Geoenviron. Eng.,* 149(7): 04023045.

Akin, I., J. Guerra, K. Hudson, M. Hudson, C. Davis, M. Fidansoy, D. Jana, S. Narasimhan, S. Tirkes, A. Sahin, S. Brandenberg, S. Moon, T. Horvath, A. Koutsoukos, D. Paige, D. Cavagnaro, D. Lindsay (2025). "Data collected from GEER response to January 2025 Los Angeles Wildfires", in GEER - 2025 Los Angeles Wildfires. DesignSafe-CI. https://doi.org/10.17603/ds2-6g0m-xn64

Atwater, T. (1998). Plate tectonic history of southern California with emphasis on the western Transverse Ranges and northern Channel Islands. In P. W. Weigand (Ed.), Contributions to the geology of the Northern Channel Islands, southern California (pp. 1–8). American Association of Petroleum Geologists. https://doi.org/10.32375/1998-mp45.1

Bailey, R.G., (1969). Soil slippage: an indicator of slope instability on chaparral watersheds of Southern California, The Professional Geographer, 21:3, 172-177, DOI: 10.1111/j.0033-0124.1969.00172.x

Brigham, C., Scott, C., Crosby, C., Beckley, M. (2025). Topographic differencing spanning the 2025 Palisades and Eaton Fires, LA. Distributed by OpenTopography. https://doi.org/10.5069/G95B00PW. Accessed: 2025-05-30

Buckley, C.L., R.A. Hollingsworth (1984). Residential Development and Landsliding, Castellammare Mesa Area, Los Angeles, California, Field Guide to Selected Engineering Geologic Features Malibu, Los Angeles County, California. Southern California Section Annual Field Trip, June 2, 1984, pp. 99-111.

CAL FIRE, 2018, California Vegetation WHRTYPE. https://www.arcgis.com/home/item.html?id=35b4d77128264b3bacd31d9685f974b7, accessed March 4, 2025.

Campbell, R.H. (1975). Soil slips, debris flows, and rainstorms in the Santa Monica Mountains and vicinity, southern California: U.S. Geological Survey Professional Paper 851, 51 p.

Cannon, S.H., Gartner, J.E., Wilson, R., Bowers, J., Laber, J. (2008). Storm rainfall conditions for floods and debris flows from recently burned areas in southwestern Colorado and southern California. Geomorphology 96, 250–269. https://doi.org/10.1016/j.geomorph.2007.03.019

Cannon, S.H., Boldt, E.M., Kean, J.W., Laber, J.L., and Staley, D.M. (2010). Relations between rainfall and postfire debris-flow and flood magnitudes for emergency-response planning, San Gabriel Mountains, southern California: U.S. Geological Survey Open–File Report 2010-1039, 31 p.

Chen, Z., Geyman, E., & Lamb, M. (2025). UAV Lidar-Based Debris Basin Capacity Assessment Following the 2025 Eaton Wildfire and the Presidents' Weekend Storm, Los Angeles County [Data set]. Zenodo. https://doi.org/10.5281/zenodo.14984875

Davis, T. L., & Namson, J. S. (1994). A balanced cross-section of the 1994 Northridge earthquake, southern California. Nature, 372, 167–169. https://doi.org/10.1038/372167a0

Dibblee Jr, T. W. (1982). Regional geology of the Transverse Ranges Province of southern California. Geology and mineral wealth of the California Transverse ranges, 10, 7-26.

Dolan, J. F., Sieh, K., & Rockwell, T. K. (2000). Late quaternary activity and seismic potential of the Santa Monica fault system, Los Angeles, California. Bulletin of the Geological Society of America, 112(10), 1559–1581. https://doi.org/10.1130/0016-7606(2000)112.

Hungr, O., Evans, S. G., Bovis, M., & Hutchinson, J. (2001). Review of the Classification of landslides of the flow type. Environmental and Engineering Geoscience. 7(3), 221-228.

Jennings, C.W., Gutierrez, C., Bryant, W., Saucedo, G., and Wills, C. (2010). Geologic map of California: California Geological Survey, Geologic Data Map No. 2, scale 1:750,000.

Kean, J. W., Staley, D. M., and Cannon S. H. (2011). In situ measurements of post-fire debris flows in southern California: Comparisons of the timing and magnitude of 24 debris-flow events with rainfall and soil moisture conditions, J. Geophys. Res., 116, F04019, doi:10.1029/2011JF002005.

Krohn, J.P. (1992). "Landslide mitigation using horizontal drains, Pacific Palisades area, Los Angeles, California." Landslides/Landslide Mitigation, J. E. Slosson, A. G. Keene, and J. A. Johnson, eds., 0. Geological Society of America.

Li, Z., and Yu, W. (2025). Economic Impact of the Los Angeles Wildfires. https://www.anderson.ucla.edu/about/centers/ucla-anderson-forecast/economic-impact-los-angeles-wildfires

Manning M (1993). A Short History of Fire and Fire Protection in Altadena, Altadena Heritage, https://altadenaheritage.org/a-short-history-of-fire-and-fire-protection-in-altadena/

Niemi, N. A., and Clark, M. K. (2017). Long-term exhumation rates exceed paleoseismic slip rates in the central Santa Monica Mountains, Los Angeles County, California. Geology. 46 (1): 63–66. doi: https://doi.org/10.1130/G39388.1

National Park Service NPS (2015). Chaparral—Santa Monica Mountains National Recreation Area. https://www.nps.gov/samo/learn/nature/chaparral.htm

Namson, J., & Davis, T. (1988). Structural transect of the western Transverse Ranges, California: Implications for lithospheric kinematics and seismic risk evaluation. Geology, 16(8), 675-679.

Perica S, Dietz S, Heim S, Hiner L, Maitaria K, Martin D, Pavlovic S, Roy I, Trypaluk C, Unruh D, Yan F. (2014). NOAA Atlas 14, precipitation-frequency Atlas of the United States, 6 (Version 2.3)[California]. National Oceanic and Atmospheric Administration, Silver Spring MD. Available at https:// hdsc.nws.noaa.gov/hdsc/pfds/index.html [Accessed 29 March 2024].

Pierson, T. C. (2005a). Hyperconcentrated flow—Transitional process between water flow and debris flow. In M. Jakob, & O. Hungr (Eds.), Debris flows and related phenomena (pp. 159–202). Heidelberg: Springer.

Pierson, T. C. (2005b). Distinguishing between debris flows and floods from field evidence in small watersheds: U.S. Geological Survey Fact Sheet 2004-3142, 4 p. Accessed 6 January 2025 at https://pubs.usgs.gov/fs/2004/3142/

Rathje, E. M., Dawson, C., Padgett, J. E., Pinelli, J., Stanzione, D., Adair, A., Arduino, P., Brandenberg, S. J., Cockerill, T., Dey, C., Esteva, M., Haan, F., Kareem, A., Lowes, L., and Mosqueda, G. (2017). DesignSafe: new cyberinfrastructure for natural hazards engineering. Natural Hazards Review, 18(3).

Rengers, F.K., McGuire, L.A., Oakley, N.S., Kean, J.W., Staley, D.M., and Tang, H. (2020). Landslides after wildfire: initiation, magnitude, and mobility: Landslides, v. 17, p. 2631–2641, https://doi.org/10.1007/s10346-020-01506-3.

Rengers, F. K., McGuire, L. A., Barnhart, K. R., Youberg, A. M., Cadol, D., Gorr, A. N., ... & Kean, J. W. (2023). The influence of large woody debris on post-wildfire debris flow sediment storage. Natural Hazards and Earth System Sciences, 23(6), 2075-2088.

Rice, R.M. and Foggin, G.T. III (1971). Effect of high intensity storms on soil slippage on mountainous watersheds in southern California: Water Resources Research, v. 7, p. 1485–1496, https://doi.org/10.1029/WR007i006p01485.

Staley, D.M., Negri, J.A., Kean, J.W., Laber, J.L., Tillery, A.C. and Youberg, A.M. (2016). Updated logistic regression equations for the calculation of postfire debris-flow likelihood in the western United States (p. 13). US Department of the Interior, US Geological Survey.

Staley, D. M., J. A. Negri, J. W. Kean, J. L. Laber, A. C. Tillery, and A. M. Youberg, A. M. (2017). Prediction of spatially explicit rainfall intensity–duration thresholds for post-fire debris-flow generation in the western United States. Geomorphology, 278:149-162. https://doi.org/10.1016/j.geomorph.2016.10.019.

Sullivan, D. (1994). Undaunted by Disaster: Pasadena Glen's Fires and Floods Are Seen as Cost of Living, Los Angeles Times, https://www.latimes.com/archives/la-xpm-1994-06-02-ga-64883-story.html

Synoptic (2025). Synoptic Data, "Weather API". Accessed 19 May 2025 at https://synopticdata.com/weatherapi/

Townsend, K. F., Clark, M. K., & Niemi, N. A. (2021). Reverse faulting within a continental plate boundary transform system. Tectonics, 40, e2021TC006916. https://doi.org/10.1029/2021TC006916

Treiman, J.A., compiler. (2000). Fault number 105d, Sierra Madre fault zone, Sierra Madre C section, in Quaternary fault and fold database of the United States: U.S. Geological Survey website, https://earthquakes.usgs.gov/hazards/qfaults, accessed 04/25/2025 09:51 AM.

URS (2010). Soil-Structure Interaction Modeling of a Landslide-Stabilization Scheme.

USACE (2025). PL 84-99 Advaced Measures, Post-Wildfire Hazard Assessment, 2025 Eaton Fire, County of Los Angeles, California, May 2025, US Army Corps of Engineers, Los Angeles District, Draft Report, 435p.

Vergani, C., Werlen, M., Conedera, M., Cohen, D., and Schwarz, M. 2017). Investigation of root reinforcement decay after a forest fire in a Scots pine (*Pinus sylvestris*) protection forest. *Forest Ecology and Management,* 400: 339-352.

Watershed Emergency Response Team (WERT) Evaluation - 2025 Palisades Fire (2025).

Watershed Emergency Response Team (WERT) Evaluation - 2025 Eaton Fire (2025).

Wolfe, D. L., 2006, Los Angeles County Department of Public Works – Hydrology Manual, January 2006, p.160.

https://dpw.lacounty.gov/wrd/publication/engineering/2006_Hydrology_Manual/2006%20Hydrolo gy%20Manual-Divided.pdf.

Wunderground, (2025). Weather Underground, "Wundermap". Accessed 19 May 2025 at https://www.wunderground.com/wundermap.

Yerkes, Robert F., and Russell H. Campbell. (1979). Stratigraphic nomenclature of the central Santa Monica Mountains, Los Angeles County, California. No. 1457. US Government Printing Office.